Efficient Förster Energy Transfer
From Phosphorescent Organic Molecules to J-aggregate Thin Film

by

Yasuhiro Shirasaki

S. B. Electrical Science and Engineering (2006)

S. B. Physics (2006)

Massachusetts Institute of Technology

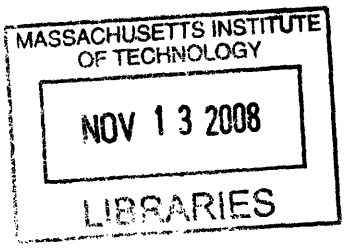

Submitted to the Department of Electrical Engineering and Computer Science

in Partial Fulfillment of the Requirements for the Degree of

Master of Engineering in Electrical Engineering and Computer Science

at the Massachusetts Institute of Technology

February 11, 2008

Author_____
Department of Electrical Engineering and Computer Science
February 11, 2008

Certified by_____
Vladimir Bulović
Thesis Supervisor

Accepted by_____
Arthur C. Smith
Chairman, Department Committee on Graduate Theses

Efficient Förster Energy Transfer
From Phosphorescent Organic Molecules to J-aggregate Thin Film

by

Yasuhiro Shirasaki

Submitted to the
Department of Electrical Engineering and Computer Science

February 11, 2008

In Partial Fulfillment of the Requirements for the Degree of
Master of Engineering in Electrical Engineering and Computer Science

ABSTRACT

This thesis demonstrates the first ever use of Förster resonance energy transfer (FRET) to increase the quantum efficiency of a electrically pumped J-aggregate light emitting device (JLED). J-aggregate thin films are highly absorptive films that have potential applications in a new class of optoelectronic devices, known as polaritonic devices. These devices, which utilize strong coupling between light and matter, include room temperature low power optical switches and low threshold lasers. Recent work has shown that a J-aggregate strong-coupling device can be powered not just optically but also electrically. However, since J aggregates are engineered for their optical and not electrical properties, exciting them electrically is very inefficient. JLED efficiency can be improved by first exciting phosphors that readily form excitons and then employing FRET to excite the J aggregates. Attaining high efficiency can make electrical pumping a viable option to power polaritonic devices.

Thesis Supervisor: Vladimir Bulović
Title: Associate Professor of Electrical Engineering

Table of Contents

Chapter 1: Introduction

Organic light emitting diodes (OLED) have become an increasingly used technology. An OLED's unique properties, including high power efficiency, low manufacturing cost, and color variety at wide viewing angles are making the OLED technology a strong contender in the display market. Just last year, Sony commercialized an 11 in. OLED display. However, OLEDs' applications are not limited to display technology. OLEDs that use aggregates of cyanine dye molecules for emission, called J-aggregate light emitting devices (JLED), can be used for novel optoelectronics known as polaritonic devices. This thesis develops a JLED that uses Förster resonance energy transfer (FRET) from organic phosphors to J aggregates to increase the device quantum efficiency. Efficient JLEDs have a strong potential in use for polaritonic devices.

Polaritonic devices are a new class of devices that are based on the coupling of photons and electron-hole pair eigenstates, a phenomenon known as strong coupling. Strong-coupling devices generally consist of an optical microcavity with an active material embedded inside. This active material, which may be an excited gas of molecules, semiconductor quantum wells, or a film of organic molecules, serves as a container for electron-hole pairs known as excitons. When the resonant photon energy of the microcavity is tuned to the energy of the excitons, an energy exchange between the two states occurs. When the rate of this energy exchange between the two states is faster than the combined rate of the photon leaving the microcavity and the excitons losing their phases, a strong coupling limit is said to be reached. The two states are no longer eigen-states of the system, and the two new eigen-states of the system become linear combinations of photon state and exciton state, separated in energy by a value referred to

as the Rabi splitting which is a measure of the strength of the coupling[1]. Applications of strong coupling in atomic and semiconductor systems have led to one-atom zero threshold lasers[2], high gain parametric amplifiers,[3] and predictions that strong coupling may play a key role in quantum information processors[4].

To become a viable technology, polaritonic devices must be powered efficiently. The primary method for powering them today is optical pumping. Devices are activated by short laser pulses. The only electrical pumping shown was by Tischler *et al.* in 2005. Tischler's device was a microcavity with a JLED embedded inside. He successfully demonstrated strong coupling with a Rabi splitting of 300meV[5], but the device efficiency was limited due to the inefficient JLED used[1]. Achieving high efficiency through electrical pumping can broaden the application of polaritonic devices and can also eliminate the use of complicated equipment such as lasers.

This thesis describes the development of a more efficient JLED for the purpose of making polaritonic devices technologically viable. Using a technique that is shown to improve OLED efficiencies, the JLED is doped with phosphors that, after being electrically excited, can FRET to the J-aggregates.

There are three main chapters following this introduction. Chapter two discusses structures used to experimentally confirm a FRET between J aggregates and $Ir(ppy)_3$, a widely known organic phosphorescent material, which will be referred to as just phosphors in the following text. Material incompatibility that arises when making the structures is discussed and resolved. Chapter three experimentally demonstrates the FRET using the structures from chapter two. Chapter four employs the energy transfer structure to make the JLED. The work done in each chapter builds on work done in the

previous chapters. Together, the chapters comprise a recipe to making a JLED that utilizes $Ir(ppy)_3$ to J aggregate FRET.

1-1: J Aggregates

J aggregates, short for Jelley aggregate, were first reported by Edwin Jelley of Kodak in 1936[6] and further studied by G. Scheibe towards the late 1930s[7]. J aggregation has been shown using various materials, especially using different types of cyanine dye molecules, and these J aggregates were primarily used to sensitize silver halides in the photographic film industry of the 20th century. A J aggregate generally refers to an aggregate of monomers that align themselves in such a way that their transition dipoles enhance each other. The proximity of these monomers, through intermolecular interactions, results in delocalization of the exciton over many monomers, which would otherwise be localized to a single monomer. This exciton delocalization exhibited by J aggregrates is akin to carrier delocalization in crystalline semiconductors, but occurs on a smaller size. The delocalization couples the transition dipoles of the monomers and their alignment results in unique optical properties: a fast radiative lifetime, a large oscillator strength of the aggregate known as superradiance and a very narrow spectral linewidth known as motional narrowing[8]. All are properties that are necessary in polaritonic devices. A cartoon of the aggregation process in solution and its effect on a PDBTC cyanine dye absorption spectrum is shown in Figure 1-1. The large peak, red-shift and the narrowing of the spectrum are some of the defining traits of J aggregation.

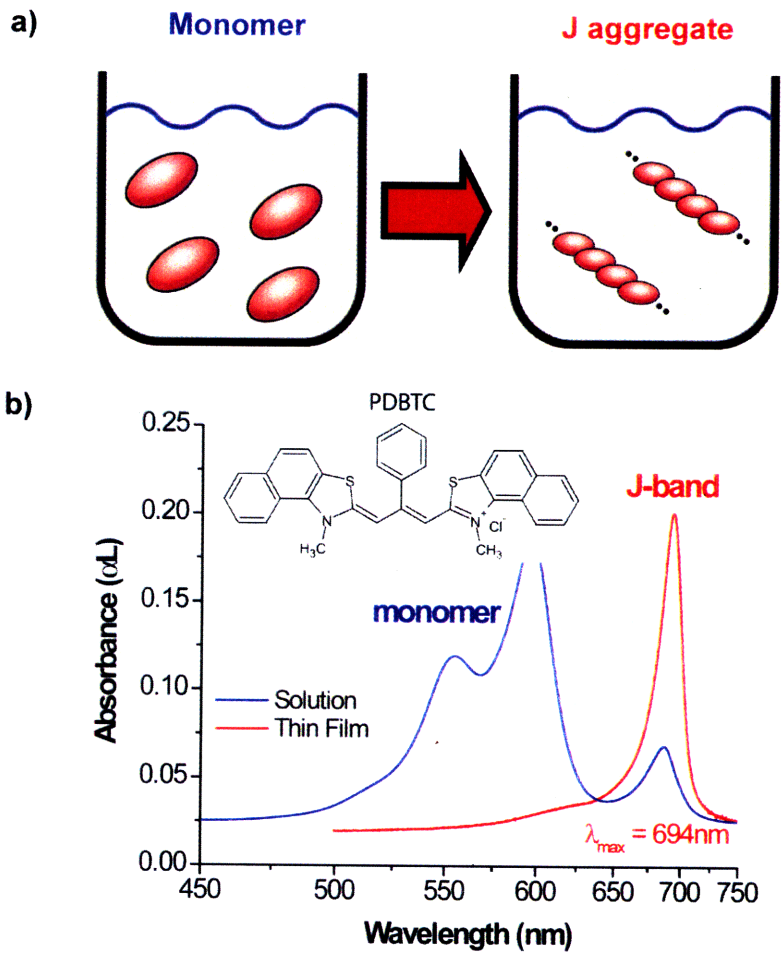

Figure 1-1: (a) Cartoon illustration of J aggregation in solution. (b) Absorption spectrums of PDBTC monomer and their J aggregates.

Recently, there has been a large interest in J aggregates for their application to polaritonic devices. J aggregates' fast radiative lifetime, small stoke shift and large oscillator strength make them appealing for use as the active material in these optoelectronic devices. In 1998, Lidzey *et al.* used J aggregates to demonstrate the strong coupling phenomenon[9]. The device was a microcavity embedded with a spun-cast film of porphyrin aggregates and a Rabi splitting of 160 meV was shown, which is an order of

magnitude larger than the 17.5 meV achieved in semiconductor systems[10]. Since then, Rabi splitting of 300 meV has been achieved using cyanine dye J aggregates[11].

Using J aggregates in polaritonic devices does not only achieve strong coupling with giant Rabi splitting, but it also allows this phenomenon to occur at room temperature which has not been possible in semiconductor systems. Due to high carrier mobility in standard semiconductor systems, without cooling to a cryogenic temperature, the effects of the input signal are quickly lost due to electronic rearrangement, known as dephasing. For these reasons, an optical microcavity with J-aggregate thin film inside has become a popular platform for studying strong coupling.

Traditionally, in active polaritonic devices, J aggregates are used in a thin film form. The film thickness varies from a few nanometers to hundreds of nanometers depending on the method of formation. The three common deposition methods are: Langmuir-Blodgett[12], spin-casting in a polymer matrix[13] and Layer-by-Layer deposition (LBL)[14]. Following Tischler's work, LBL is the method of choice in this research. Highly absorptive thin films (α=1x10^6 cm^{-1}) of TDBC J aggregates can be grown using LBL[15].

1-2: Layer-by-Layer Deposition

Layer-by-Layer deposition (LBL) is a technique for growth of nanometer scale films by sequential immersions into polycationic and polyanionic solutions. The method was first reported by Decher *et al.* in 1991[16] and has since been widely used.

LBL starts with the preparation of a starting substrate and two solutions containing oppositely charged, dissolved ionic molecules that will comprise the resulting film. One solution contains cations; the other contains anions. The substrate undergoes sequential immersion into these cationic and anionic solutions (SICAs), adsorbing a monolayer of cations or anions with each dip. The force that makes this adsorption possible is the electrostatic attraction between the ions. Every time the film is immersed in one of the two solutions, the ions adsorbs onto the surface and inverts the surface charge in the process. This charge inversion then prepares the film for the immersion in the other solution. The film is rinsed, typically with the same solvent used to prepare the ionic solutions, after each immersion into either of the solutions to wash off excess ions that stick onto the film. By repeating the number of SICAs, the film can be grown monolayer by monolayer.

Although LBL is usually performed with two kinds of strong polyelectrolytes, which are polymers with charges that are insensitive to pH, it was shown in the 1990s that one of these polyelectrolytes can be replaced with dye molecules or other small molecules with the ionic behavior[17]. These small molecules, however, must be able to sufficiently adsorb onto the film to cause the surface charge reversal. This requirement is often satisfied if the molecules are multivalent. In 1998, Fukumoto *et al.* showed that a J-aggregate thin film can be formed by replacing the polyanion with J-aggregating cyanine dye molecules in the LBL method[14].

Thorough study of LBL deposited TDBC J-aggregate thin film has been done by Bradley *et al.* His study shows the film quality, which is measured by the amount of aggregates in the film and the roughness of the film, of a 4.5 bilayer (BL) is most suited

for polaritonic devices[15]. Therefore, the 4.5 BL TDBC J-aggregate thin films are used in this research.

1-3: Energy Transfer

There are three primary mechanisms for energy transfer between molecules: radiative energy transfer via photons, Dexter energy transfer, and Förster resonance energy transfer. The first process is a long range energy transfer between molecules mediated by photons. In other words, an excited donor molecule emits a photon which is then absorbed by an acceptor molecule. Dexter energy transfer refers to the short range, non-radiative energy transfer that is caused by the wave-function overlap of the molecules[18]. This energy transfer only occurs between two adjacent molecules and intermolecular electron exchange accompanies the transfer. Förster resonance energy transfer (FRET), is a long range, non-radiative energy transfer mechanism caused by dipole-dipole coupling of the donor and acceptor molecules[19]. FRET can typically occur over a few nanometers.

FRET is used in this research because it offers energy transfer over a longer range than the Dexter energy transfer and it is more efficient than the radiative energy transfer. Radiative energy transfer is not desirable because the energy is wasted if the photons emitted from the donor molecules do not propagate in the direction of the acceptor molecules or do not get absorbed by them. FRET involving phosphorescent donors is particularly desirable. If phosphorescent donors are used, both the singlet and triplet exciton energies of the donor can be transferred to the acceptor. When an exciton forms

on a donor molecule, it is a triplet 75% and a singlet 25% of the time due to spin statistics. Unlike fluorophores that only emit photons from singlet excitons, phosphors have a heavy transition metal core that allows radiative triplet relaxation through spin-orbital coupling. Since the J aggregates in this study have a very short luminescence lifetime (~10 ps) and do not have heavy transition metals in the structure, they are not likely to be phosphors. Therefore, the J aggregates can not convert triplet excitons into photons and the luminescence efficiency is limited. Using FRET from phosphorescent donors to excite singlet excitons on the J aggregates allows for extended excitation of the J aggregrate.

The rate at which the energy is transferred from the donor to the acceptor, referred to as the FRET rate, is given by

$$\Gamma = \frac{3}{4\pi}\frac{c^4}{n^4}\frac{1}{R^6}\frac{1}{\tau}\int\frac{S_D(\omega)\sigma_A(\omega)}{\omega^4}d\omega \qquad \text{(Eq. 1-1)}$$

where c is the speed of light in vacuum, n is the index of refraction of the medium, R is the distance between the donor and acceptor molecules, τ is the luminescence decay time of the donor molecule, $S_D(\omega)$ is the normalized emission spectrum of the donor, and $\sigma_A(\omega)$ is the absorption cross-section of the acceptor. Eq. 1-1 is a result of Fermi's Golden rule applied to a system where one molecule (the acceptor molecule) is perturbed by the dipole field of a neighboring molecule (the donor molecule). The perturbation Hamiltonian is proportional to $1/R^3$, the dipole field. Fermi's Golden rule states that the energy transfer rate is proportional to the square of the perturbation Hamiltonian, resulting in one of the key features of FRET, the $1/R^6$ dependence. The spectral overlap is the result of the donor and acceptor molecules having a number of states that can donate or accept exciton energies.

One of the most important device applications of FRET in the 1990s was its application to OLEDs. A platinium octaethylporphyrin (PtOEP)

LED that utilizes efficient energy transfer was reported by Baldo *et al.* in 1998[20]. Today, PtOEP and phenylpyridine iridium complexes such as $Ir(ppy)_3$ are the most widely used phosphorescent OLED materials[21]. $Ir(ppy)_3$ has also been shown to enhance photoluminescence (PL) of quantum dots via FRET[22] and here it is used to enhance PL of the J aggregates.

Chapter 2: Growth of the FRET Devices

This chapter is the first of three chapters on the research portion of this thesis. The first step in this research is demonstrating FRET between the donor, *fac* tris(2-phenylpyridine) iridium ($Ir(ppy)_3$), and the acceptor, TDBC J aggregate.

2-1: Device Structure

The device structure and materials used to demonstrate FRET are shown in Figure 3-1. The structure consists of three organic layers on a glass substrate as shown. The bottom layer is the acceptor layer, a 5nm J-aggregate thin film grown on glass using the LBL method. The experimental details of the J aggregate growth process are given in Appendix A. The middle layer is a thermally evaporated spacer layer, which consisted of either 0, 4, or 8 nm of *p*-bis(triphenylsilyl)benzene (UGH2). UGH2 is a wide bandgap material (E_g = 4.4 eV) that does not absorb in the visible spectrum. It was used as the host material to make blue LEDs by Ren *et al.* in 2004[23]. UGH2 was chosen out of many wide bandgap materials available (such as TAZ and CBP) for its stability. Thermally evaporated films are amorphous and often times unstable, resulting in crystallization or other morphological changes. Since the spacer layer thickness needs to be uniform and well controlled for this experiment, a stable material such as UGH2 was chosen. The top layer is the thermally co-evaporated donor layer, 5 nm $Ir(ppy)_3$ (E_g = 3 eV) doped into UGH2 (~10% by volume). The chemical structure of each material is shown in Figure 3-2.

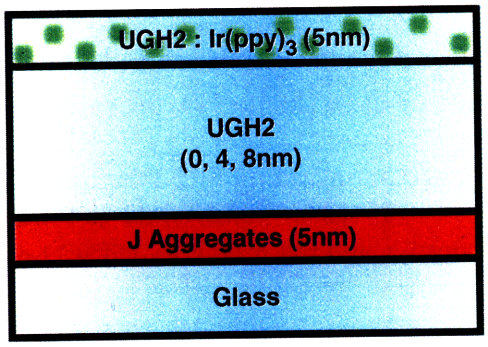

Figure 2-1: Device structure consists of 5 nm $Ir(ppy)_3$ doped in UGH2 (donor), 4, 8 or 12nm UGH2 (spacer), and 5 nm J-aggregate thin film (acceptor).

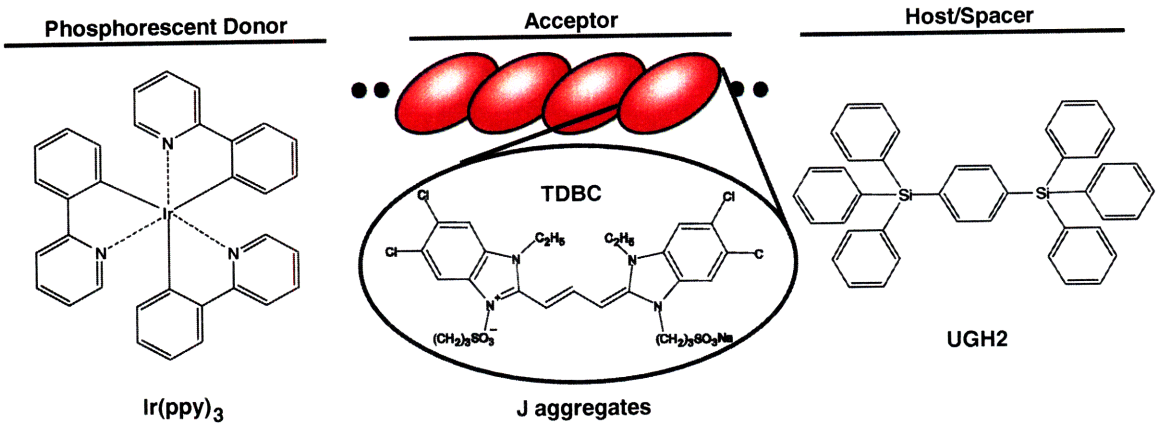

Figure 2-2: Materials used in the device

The device structure shown in Figure 3-1 is very similar to the one used by Andrew *et al.* to measure the Förster radius between a europium complex and a different kind of cyanine dye molecule[24]. However, unlike the structure used by Andrew, the structure used here does not use LB to form monolayer acceptor and donor layers. The thermal evaporation and LBL result in more than a monolayer of molecules. Although thicker acceptor and donor layers in the device presented here complicate the modeling of

the structure, they yield more signal, increasing the signal to noise ratio when measuring the PL.

Structures were grown with three different spacer layer thicknesses to demonstrate that quenching of the donor photoluminescence (PL) is strongly dependent on the distance between the donor and acceptor layers. If donor and acceptor layers are in direct contact, the dipole coupling of the molecules is so strong that the FRET rate is much faster than the exciton decay rate of the donor molecules alone. This fast FRET rate results in large portion of the donor energy getting quenched by the acceptor, and PL comes only from the acceptor. If the two layers are far apart, the dipole coupling is very weak and only PL from the donor is observed. At the Förster radius, where the FRET rate is equal to the PL decay rate, PL is expected to be observed from both the donor and acceptor layers. The theoretical Förster radius, calculated from the emission spectrum of $Ir(ppy)_3$ and the absorption spectrum of TDBC J aggregate, is 3.8 nm. The calculation details are given in Appendix B. From this theoretical value for Förster radius, spacer layer thicknesses of 0, 4, and 8 nm were chosen to observe progressive quenching of donor luminescence..

Having three thickenesses is also important in order to show that FRET - and not simply radiative energy transfer - is occurring. Since the J-aggregate thin film is highly absorptive, some radiative energy transfer can occur with the J aggregates absorbing photons given off by $Ir(ppy)_3$. With three different thicknesses, the FRET rate can be shown to be dependent on the spacer distance by comparing the PL life times of these devices. As will be shown in chapter three, the occurrence of FRET will be reflected by

accelerated lifetimes of the donor PL. Radiative energy transfer, on the other hand, does not modify the PL life times.

2-2: Problem of Material Incompatibility

The FRET rate from a single donor molecule to a film of acceptor molecules is given in Eq. 2-1 (derivation is given in chapter three). The equation is used to simulate the dependence of the fraction of donor PL that is quenched due to the presence of an acceptor on the spacer thickness. Figure 2-3 plots the dependence when the acceptor layer is 5.1 nm and the R_F is 4 nm.

$$K_{FRET} = \int_0^{d_A} K_{D\to plane}(R+z)dz = \frac{\pi\rho_A R_F^6}{6\tau}\left(\frac{1}{R^3} - \frac{1}{(R+d_A)^3}\right) \qquad \text{(Eq. 2-1)}$$

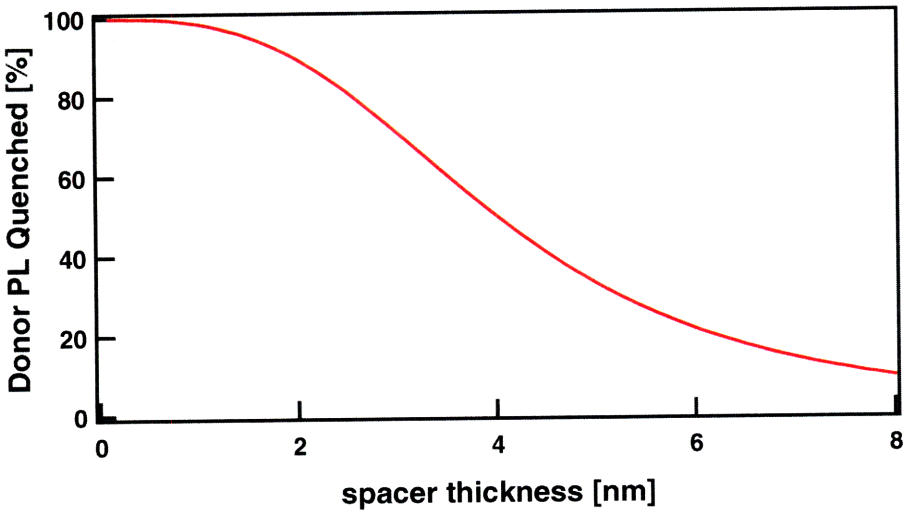

Figure 2-3: The fraction of donor PL quenched by an accepter layer.

The figure suggests the spacer layers need to be grown with nanometer scale control, especially for the 4 nm spacer layer sample. To test if this precise control was achieved, 5 nm of UGH2 was thermally evaporated on top of the J-aggregate film and the film morphology was measured using the atomic force microscope (AFM). The AFM image of this sample and that of the underlying J-aggregate film are shown in Figure 2-4. The quality of the films is characterized by their Z ranges and roughness root-mean-squares (RMS). The Z range is the distance between the lowest and the highest point of the film and the roughness RMS is the standard deviation of the height of the film. In the images, UGH2 film has a Z range of 88.8 nm and a roughness RMS of 12.5 nm while the underlying J-aggregate film has a Z range of 10.8 nm and a RMS of 1.0 nm. Both the Z range and the RMS have increased after depositing UGH2 and the precise control of the film thickness is not achieved. From their chemical structures, it can be seen that UGH2 is a non-polar molecule while J aggregates are polar. The two materials repel akin to water and oil, making uniform evaporation of UGH2 difficult. This material incompatibility issue must be solved in order to make the desired structures.

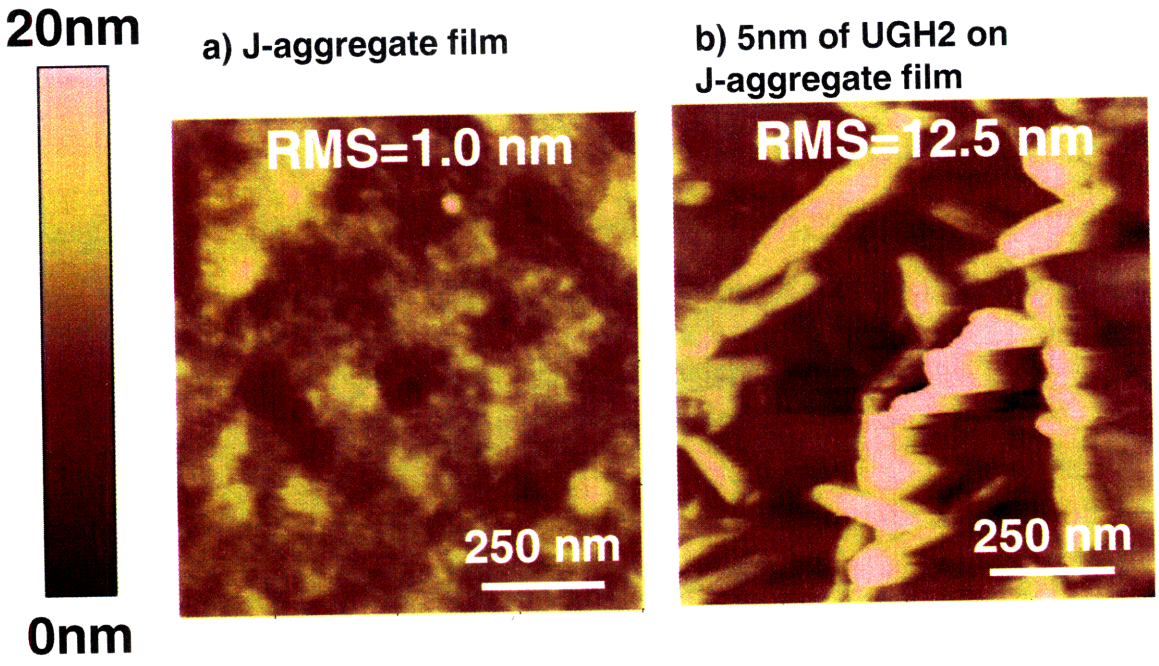

Figure 2-4: (a) AFM image of 4.5 BL J-aggregate thin film. (b) AFM image of 5 nm of UGH2 thermally evaporated on the J-aggregate film.

2-3: Solution to the Material Incompatibility

The solution to the material incompatibility demonstrated here resolves the delamination of UGH2 from the J-aggregate film and allows incorporation of J-aggregate thin films in device structures with non-polar small molecules.

Just as soap is used to bring water and oil together, a surfactant is used to bring together polar J aggregates and non-polar UGH2. A surfactant molecule is a molecule that is hydrophilic on one end and hydrophobic on the other end. The hydrophilic end can be a polar molecule or an ion. The hydrophobic end is generally a hydrocarbon chain(s). By aligning the surfactant molecules between the J aggregates and UGH2 so the hydrophilic ends face the J aggregates and the hydrophobic ends face UGH2, the two materials can be placed in proximity.

There are three steps to the surface treatment recipe to make the hydrophilic surface hydrophobic, outlined below. It will be followed by an analysis of the film. A discussion of alternative methods and materials that were tried is provided in Appendix C. While they did not provide the desired results, they revealed some important properties of the J-aggregate film.

2-3a: Surface Treatment

Step 1: The 4.5 BL J-aggregate thin film is immersed in 0.03M solution of Sodium Polystyrene Sulfonate (SPS) for 1 minute and then rinsed off with de-ionized (DI) water. SPS is a strong polyanionic electrolyte that is commonly used for LBL method to make novel, nano-structured thin films[25]. Since our J-aggregate film ends with a PDAC deposition, the surface is positively charged. Immersion into SPS solution adds a monolayer of SPS molecules on the surface, via electrostatic attraction, while inverting the surface charge from positive to negative. A cartoon illustration of step 1 is shown in Figure 2-5.

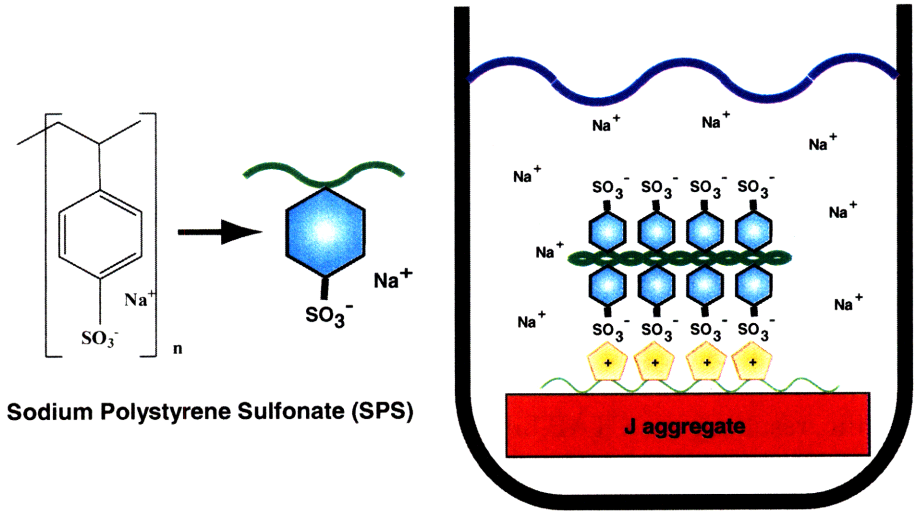

Figure 2-5: Immersion of the J-aggregate film into a SPS solution.

Step 2: The resulting film is immersed in 0.01M solution of cetyl trimethylammonium bromide (CTAB) for 10min and then rinsed off with DI water. CTAB is a cationic surfactant that performs as the glue between the SPS surface and UGH2. The concentration of CTAB was chosen to be much higher than the concentration needed to form aggregates of CTAB (1.0mM), known as the critical micelle concentration (CMC). The high concentration ensures CTAB's complete coverage of the film. A cartoon illustration of step 2 is shown in Figure 2-6.

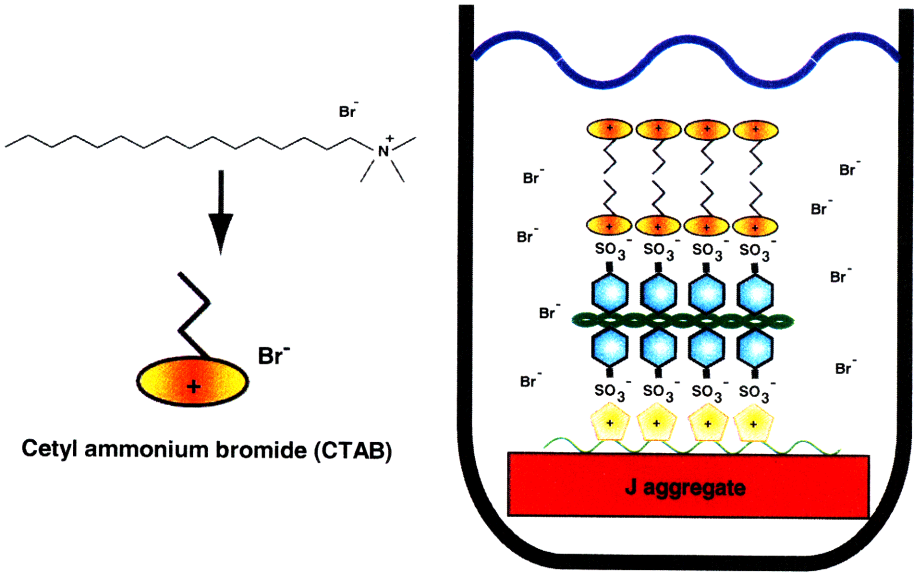

Figure 2-6: Immersion of the film into a CTAB solution.

Step 3: The resulting film is rinsed off in chloroform for 5 seconds. This step washes off all the CTAB molecules except a single monolayer that is electrostatically bound to the SPS molecules. Chloroform is used instead of DI water here because it is a small molecule and is an organic solvent. Washing off with DI water likely leaves the film surface hydrophilic, resulting in a CTAB bilayer similar to the lipid bilayers found in cell membranes. The small size of chloroform allows it to penetrate through the outer layer of this bilayer and its organic-like property allows it to break off the outer layer. Blow

drying the film with nitrogen gas leaves the hydrocarbon chains of CTAB pointing outwards, making the film surface hydrophobic. A cartoon illustration of the step 3 is shown in Figure 2-7.

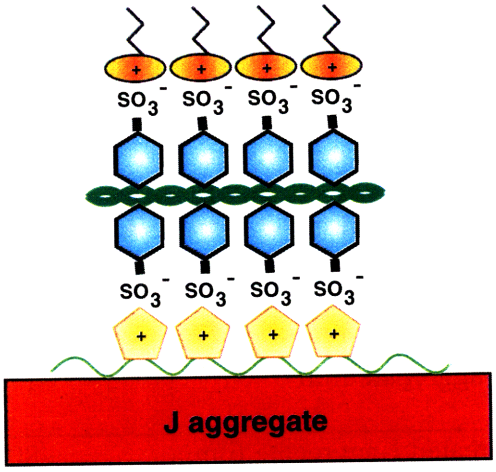

Figure 2-7: Film after the surface treatment.

2-3b: Contact Angle Measurements

The effect of the surface treatment is measured by conducting a contact angle measurement. A droplet of DI water is dropped on the film from a syringe placed ~5mm above the film. The angle the droplet makes with the surface is measured. Schematic of this measurement is shown in Figure 2-8.

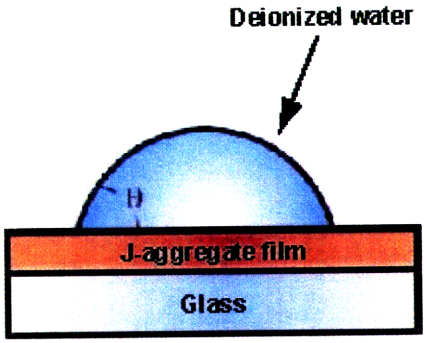

Figure 2-8: Contact angle measurement

A large contact angle indicates that the surface is hydrophobic. Contact angles for a glass substrate, the J-aggregate film, and the film with the surface treatment are given in Table 2-1. The contact angle of untreated J-aggregate film is ~17°, which is only slightly more hydrophobic than glass. The surface treatment boosts this contact angle of the J-aggregate film to ~80°, indicating the success of making the surface hydrophobic.

Material	**Contact Angle, θ**
Glass (oxygen plasma treated)	~5°
J-aggregate film	~17°
Surface Treated J-aggregate film	~80°

Table 2-1: Contact angle measurements on various substrates

2-3c: Thermally Evaporated UGH2 on Surface Treated J-Aggregate Thin Film

Our hypothesis that a hydrophobic surface allows for more uniform growth of UGH2 is investigated by comparing the AFM-measured RMS roughness of (a) an untreated J-aggregate film, (b) a surface treated J-aggregate film, (c) 5 nm of UGH2 thermally evaporated on an untreated J-aggregate film, and (d) 5 nm of UGH2 on a surface treated J-aggregate film (See Figure 2-9). Surface treatment of the J-aggregate film increases the RMS from 1.0 nm to 1.8 nm. This may be due to the adsorbed CTAB not forming a complete monolayer. However, comparing the AFMs in (c) and (d) clearly shows that surface treatment improved the uniformity of UGH2 on J-aggregate. The RMS roughness is reduced from 12.5 nm to 1.9 nm because the pillar-like aggregates of

UGH2 are not present with the surface treated structure. Elimination of these pillars is important because they are likely to cause shorts or instability in a JLED. The surface treatment developed here is therefore crucial not only for the energy transfer experiments but also for device fabrication. Indeed, the same treatment will be applied to building JLEDs in chapter four.

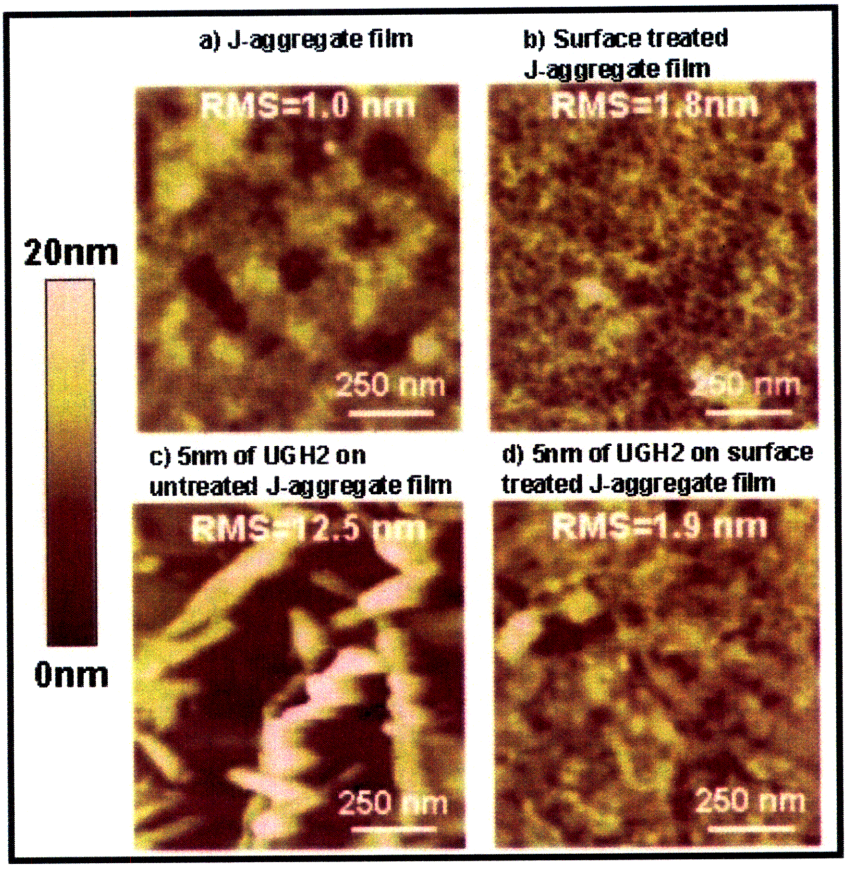

Figure 2-9: AFM images of (a) 4.5 BL J-aggregate thin film. (b) surface treated J-aggregate film. (c) 5 nm UGH2 on untreated J-aggregate film. (d) 5 nm UGH2 on surface treated J-aggregate film.

For use in potential devices and to test the robustness of the surface treatment, 5 nm of N,N'-Bis(3-methylphenyl)-N,N'-bis-(phenyl)-9,9-spiro-bifluorenes (spiro-TPD), another wide bandgap material, was thermally evaporated on untreated and surface

treated J-aggregate films. Their AFM images are shown in Figure 2-10. Without the surface treatment, spiro-TPD forms tall pillars and barely covers the surface of the J-aggregate film. The RMS of the spiro-TPD film is reduced from 8.25 nm to 2.28 nm after the surface treatment. Although the effect is not as drastic as the effect observed with UGH2, the surface treatment proves to be effective.

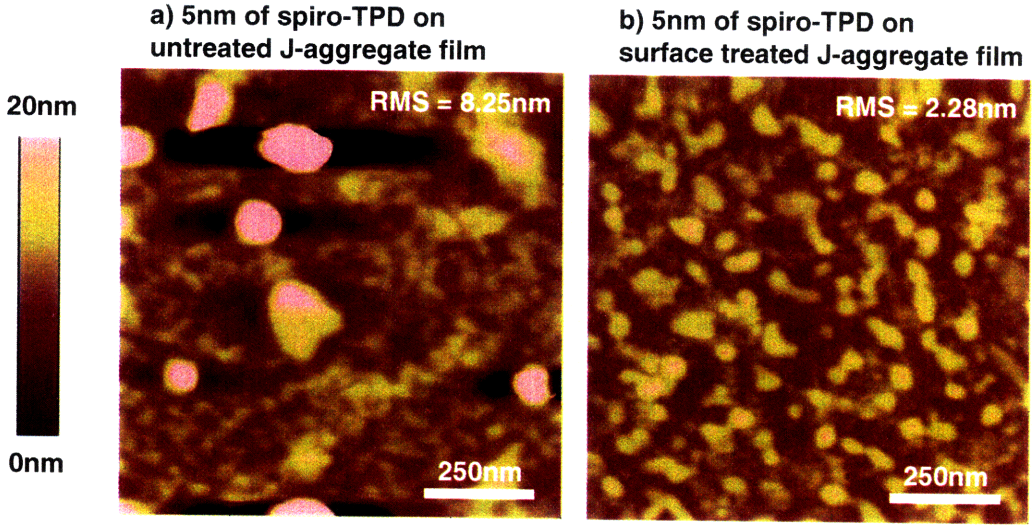

Figure 2-10: AFM images of (a) 5 nm spiro-TPD on untreated J-aggregate film. (b) 5 nm spiro-TPD on surface treated J-aggregate film

2-3d: Surface Treatment Thickness

The thickness of the layer adsorbed by the surface treatment was determined using the Gaertner Scientific 3-Wavelength Variable Angle Ellipsometer. An 830 nm light source was used to avoid absorption by the J aggregates. First, the thickness of a J-aggregate film was measured with the ellipsometer. The thickness of the same film was measured again after the surface treatment. The difference in the thicknesses was determined to be the thickness of the surface treatment. Since the resolution of the

ellipsometer does not permit the use of 4.5 BL J-aggregate thin film (corresponds to ~5 nm), 8.5BL J-aggregate film (~10 nm) was used instead. After averaging five measurements, the thickness of the film adsorbed by the surface treatment (SPS and CTAB layers) was determined to be 1.74 nm.

Chapter 3: Demonstration of FRET

This chapter provides the result of the experiment to verify Förster energy transfer between $Ir(ppy)_3$ molecules and the J aggregates. The devices prepared in the previous chapter (Figure 2-1) are optically excited, from the donor layer side, with 150 fs laser pulses tuned at 395 nm. The opitcal source used is a Ti-sapphire laser. Photoluminescence from the donor side of the samples is collected using a lens and detected with a streak camera with a 1 μs time window. A schematic of the setup is shown in Figure 3-1.

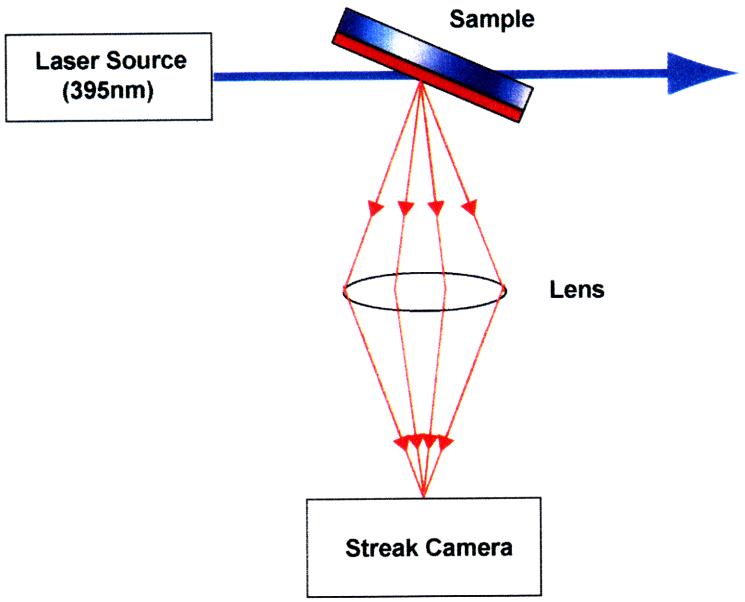

Figure 3-1: Schematic of the time-resolved PL experiment setup.

Prior to exciting the samples, each sample was packaged to prevent degradation of the organic materials. For packaging, glass microscope cover slips were glued onto the samples using UV-curable epoxy in a nitrogen environment.

3-1: Result

Figure 3-2 compares the streak camera photoluminescence of five different samples consisting of: (1) 4 nm thermally evaporated $Ir(ppy)_3$:UGH2, (2) 4.5 BL of surface-treated J-aggregate film, (3) 4.5 BL of surface-treated J-aggregate film, an 8 nm UGH2 spacer layer, and 5 nm $Ir(ppy)_3$:UGH2, (4) 4.5 BL of surface-treated J-aggregate film, a 4 nm UGH2 spacer layer, and 5 nm $Ir(ppy)_3$:UGH2, and (5) 4.5 BL of surface-treated J-aggregate film, and 5 nm $Ir(ppy)_3$:UGH2. The $Ir(ppy)_3$ sample exhibits a PL lifetime of 520 ns. This lifetime is short for a phosphor, but it is consistent with previous measurements made by Baldo *et al.*[26]. The $Ir(ppy)_3$ emission peak is at 515 nm. The J-aggregate film has a lifetime shorter than what can be resolved in the measurement setup. A lifetime of 10 ps was attained from a pump probe experiment by Zhang *et al.*[27]. The emission peak of the J aggregates is observed at 590 nm. The three samples with different spacer layer thicknesses show emission from both the donor ($Ir(ppy)_3$) and the acceptor (J-aggregate). A thick spacer layer results in higher fraction of PL from the $Ir(ppy)_3$ while a thin spacer results in PL spectrum dominated by the J aggregates. A change in the lifetime from device to device is also apparent, indicating the presence of FRET.

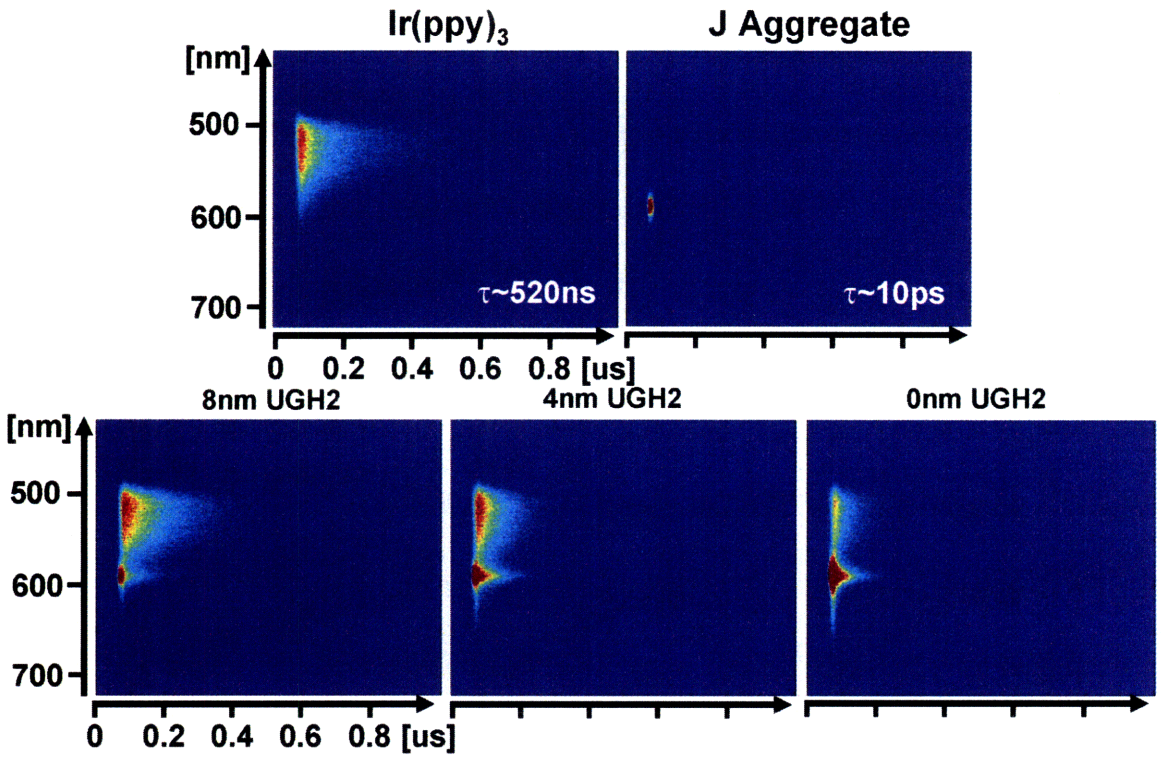

Figure 3-2: Streak camera pictures of PL from (a) $Ir(ppy)_3$ (b) J aggregates (c) J aggregates-8 nm UGH2- $Ir(ppy)_3$ (d) J aggregates-4 nm UGH2- $Ir(ppy)_3$ (e) J aggregates-0 nm UGH2- $Ir(ppy)_3$

The streak camera data is integrated over time to obtain the distribution of photon wavelengths emitted from the samples. This integration gives the graph shown in Figure 3-3. Again, J-aggregate PL is stronger when the spacer layer is thinner. The device with 8 nm of UGH2 still exhibits J-aggregate PL despite the acceptor layer being located much farther than the Förster radius away from the donor layer. Most of this J-aggregate PL is attributed to the direct excitation of the J-aggregate layer by the laser pulse. Although some of this PL maybe be due to radiative energy transfer between the $Ir(ppy)_3$ and the J aggregates, it is considered to be negligible because the J-aggregate layer is very thin and the internal quantum efficiency of the J-aggregate film is assumed to be low. The 0 nm UGH2 sample still shows PL from $Ir(ppy)_3$. This PL is attributed to the thick donor layer,

resulting in some $Ir(ppy)_3$ molecules being farther away from the acceptor layer than the Förster radius. The 1.74 nm layer from the surface treatment also adds to this effect.

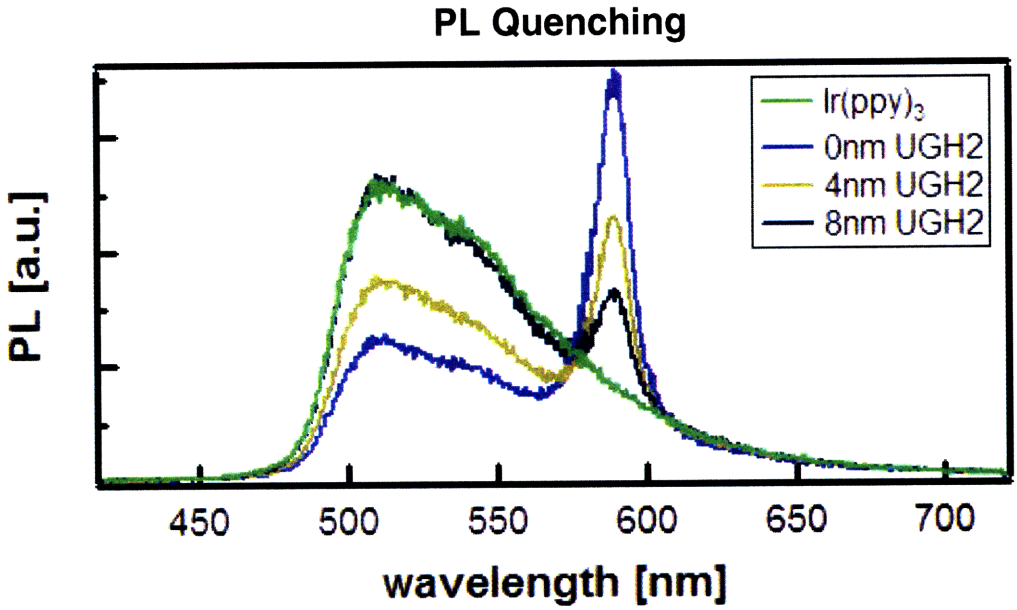

Figure 3-3: PL spectrum of the 4 samples.

Although the change in the quenching ratio is suggestive of FRET, it alone is not definitive. As discussed in chapter two, a more direct confirmation of FRET is observing the change in radiative lifetime of the samples as a function of the spacer layer thickness. Effective radiative lifetime, τ_{eff}, of an exciton can be given by:

$$\frac{1}{\tau_{eff}} = \Gamma_{rad} + \Gamma_{non-rad} + K_{FRET} = \frac{1}{\tau} + K_{FRET} \qquad \text{(Eq. 3-1)}$$

Γ_{rad} is the rate that an exciton turns into a photon without any other loss processes. $\Gamma_{non-rad}$ is the rate that an exciton loses its energy via a non-radiative mechanism. This process includes excitons turning into phonons through interactions with phonons. The two rates combined gives the natural lifetime of the exciton, $1/\tau$. K_{FRET} is the FRET rate of the donors in the presence of an acceptor molecule(s). Hence, presence of acceptor molecules shortens the lifetime of the excitons. As predicted, Figure 3-4 shows

accelerated PL for samples with the donor layers; the samples with thinner spacer layer show more acceleration. This confirms the presence of FRET in the samples.

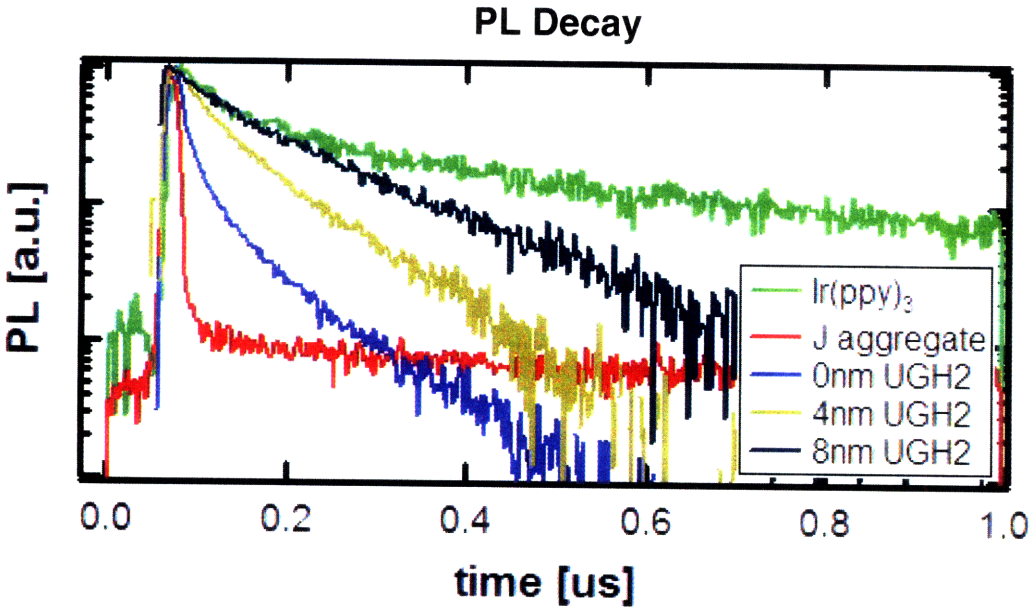

Figure 3-4: PL decay plots of the 4 samples in a semi-log scale.

3-2: Measured Förster Radius

From the PL quenching graphs, the Förster radius can be experimentally obtained. The device structure is shown again in Figure 3-5.

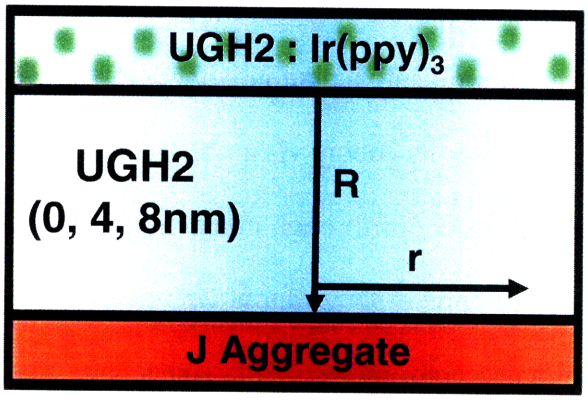

Figure 3-5: Energy transfer device structure.

The FRET rate, K_{FRET}, can be related to the donor PL by:

$$\frac{\#Ir(ppy)_3\,photons_{DA}}{\#Ir(ppy)_3\,photons_D} = \frac{\Gamma_{rad}+\Gamma_{non-rad}}{\Gamma_{rad}+\Gamma_{non-rad}+K} = \frac{1}{1+\tau K_{FRET}} \qquad \text{(Eq. 3-2)}$$

$\#\ Ir(ppy)_3\ photons_{DA}$ is the number of photons from $Ir(ppy)_3$ in presence of acceptors and $\#\ Ir(ppy)_3\ photons_D$ is the number of photons from $Ir(ppy)_3$ without any acceptors present. Since the donor layer has a finite thickness, Eq. 3-2 is averaged over its thickness, d_D. The averaging is done under the assumption that the exciton population in the donor layer is uniform upon excitation. This assumption can be made because $Ir(ppy)_3$ excitons have a relatively slow diffusion rate[22]. If the diffusion is negligible, then the donor film can be modeled as a stack of many thin donor layers.

$$\frac{\#Ir(ppy)_3\,photons_{DA}}{\#Ir(ppy)_3\,photons_D} = \frac{1}{d_D}\int_{R=0}^{R=d_D}\frac{1}{1+\tau K_{D\to film}(R)}dR \qquad \text{(Eq. 3-3)}$$

$K_{D\to film}$ is the FRET rate from a single donor molecule to a film of acceptor molecules. This rate is calculated by first integrating over a plane the FRET rate from a single donor molecule to a single acceptor molecule, $K_{D\to A}$. The result is the FRET rate from a single donor molecule to a plane of acceptor molecules, $K_{D\to plane}$. $K_{D\to plane}$ is integrated over the thickness of the acceptor film to obtain $K_{D\to film}$.

$$K_{D\to A}(R) = \frac{1}{\tau}\left(\frac{R_F}{R}\right)^6 \qquad \text{(Eq. 3-4a)}$$

$$K_{D\to plane}(R) = \int_0^\infty \frac{1}{\tau}\frac{R_F^6}{(R^2+r^2)^3}\times 2\pi r\rho_A dr = \frac{\pi\rho_A}{2\tau}\frac{R_F^6}{R^4} \qquad \text{(Eq. 3-4b)}$$

$$K_{D\to film} = \int_0^{d_A} K_{D\to plane}(R+z)dz = \frac{\pi\rho_A R_F^6}{6\tau}\left(\frac{1}{R^3}-\frac{1}{(R+d_A)^3}\right) \qquad \text{(Eq. 3-4c)}$$

Here, d_A is the thickness of the acceptor layer and ρ_A is the density of the acceptor molecules in the film. R is taken to be the sum of the 1.74 nm from the surface treatment

and the UGH2 spacer layer thickness (i.e. 0, 4, or 8 nm). R_F is calculated from relating Eq. 3-3 and Eq. 3-4c. The result is given in Table 3-1.

Sample	Calculated R_F [nm]
0nm UGH2	3.81 ± 0.13
4nm UGH2	4.46 ± 0.29
8nm UGH2	3.81 ± 0.99
Predicted R_F	3.8

Table 3-1: Calculated and predicted Förster radius.

Table 3-1 shows that the calculated Förster Radii are in good agreement with the value predicted from the $Ir(ppy)_3$ and J aggregate spectral overlap. The error bars are large due to the inherent roughness of the films.

The results presented in this chapter confirm FRET between $Ir(ppy)_3$ molecules and J aggregates.

Chapter 4: Application of FRET to a J-aggregate Light Emitting Device

The chapter applies the FRET between $Ir(ppy)_3$ molecules and J aggregates to make a J-aggregate light emitting device (JLED) that is more efficient than the same JLED without FRET. Efficient JLEDs can lead to electrically pumped polaritonic devices in the future. Here we report the first JLED that incorporates p-type metal oxide and utilizes FRET from a phosphor. Peak efficiency of the device is ~0.001%.

4-1: JLED

Four different device structures were grown in this experiment. Their device structures and their band diagrams are shown in Figure 4-1. All devices are grown on 1in. x 1in. indium tin oxide (ITO) substrates, which serve as the anodes. The cathodes are thermally evaporated 20 nm of magnesium and silver alloy capped with 100 nm of pure silver. The electron transporting layer (ETL) is 1,3,5-tris(2-N-phenylbenzimidazolyl)benzene (TPBi) which was chosen for its relatively wide bandgap and the alignment of the LUMO band with UGH2's LUMO band. The hole transporting layer (HTL) is 20 nm of sputtered nickel oxide (NiO). NiO HTL is motivated by its successful use to make quantum dot LED by Caruge *et al.* in 2006[28]. While NiO is normally an insulating metal oxide, it can be made p-type by controlling the oxygen partial pressure during the oxide growth. Sputtering with a surplus of oxygen fills oxygen vacancies, leaving two holes that contribute to the p-type conduction. This process can be expressed using the Kroger-Vink notation[29]:

$$\frac{1}{2}O_2 + V_O^{\bullet\bullet} \rightarrow O_O + 2h^{\bullet} \qquad \text{(Eq. 4-1)}$$

Material properties and the growth conditions of NiO are investigated and reported by Wood[30]. Use of metal oxides is one of the improvements suggested in Tischler's work on JLEDs. Metal oxides are promising material for JLEDs because they are not only transparent and offer tunable conductivity, but are also relatively stable in water[31]. Growth of J aggregates out of solution requires the underlying substrate to be dipped in water, which causes rapid degradation of most organics. Metal oxides offer a stable charge transport layer for J aggregate deposition.

Device 1 is the test structure that uses TPBi as both the ETL and the emissive layer. Device 2 is the $Ir(ppy)_3$ LED that incorporates $Ir(ppy)_3$ and UGH2. $Ir(ppy)_3$ and UGH2 are thermally co-evaporated (~10% by volume) for 4 nm as was done in chapter two. An additional 6 nm of UGH2 is evaporated on top. While UGH2 is a good host material for $Ir(ppy)_3$, UGH2 also serves as a hole blocking layer that blocks holes from NiO layer and prevents exciton recombination in the TPBi layer. Device 3 is the JLED that utilizes FRET from $Ir(ppy)_3$. The device is identical to Device 2 except the 4.5 BL J-aggregate film is grown on NiO. The J-aggregate deposition is followed by the surface treatment developed in chapter two. The growth procedure of the J-aggregate film is same as that described in Appendix A, but the initial oxygen plasma step is omitted. The step was omitted because the oxygen plasma may modify the sputtered NiO layer and therefore change its properties, such as its conductivity. The values of the lowest unoccupied molecular orbital (LUMO) and the highest occupied molecular orbital (HOMO) bands of the J-aggregate film are not known but the film is assumed to not substantially effect the conduction of electrons and holes through the device due to the J-

aggregate layer thinness. Device 3 is compared with Device 4, a same structure as Device 3 but without the $Ir(ppy)_3$ doping.

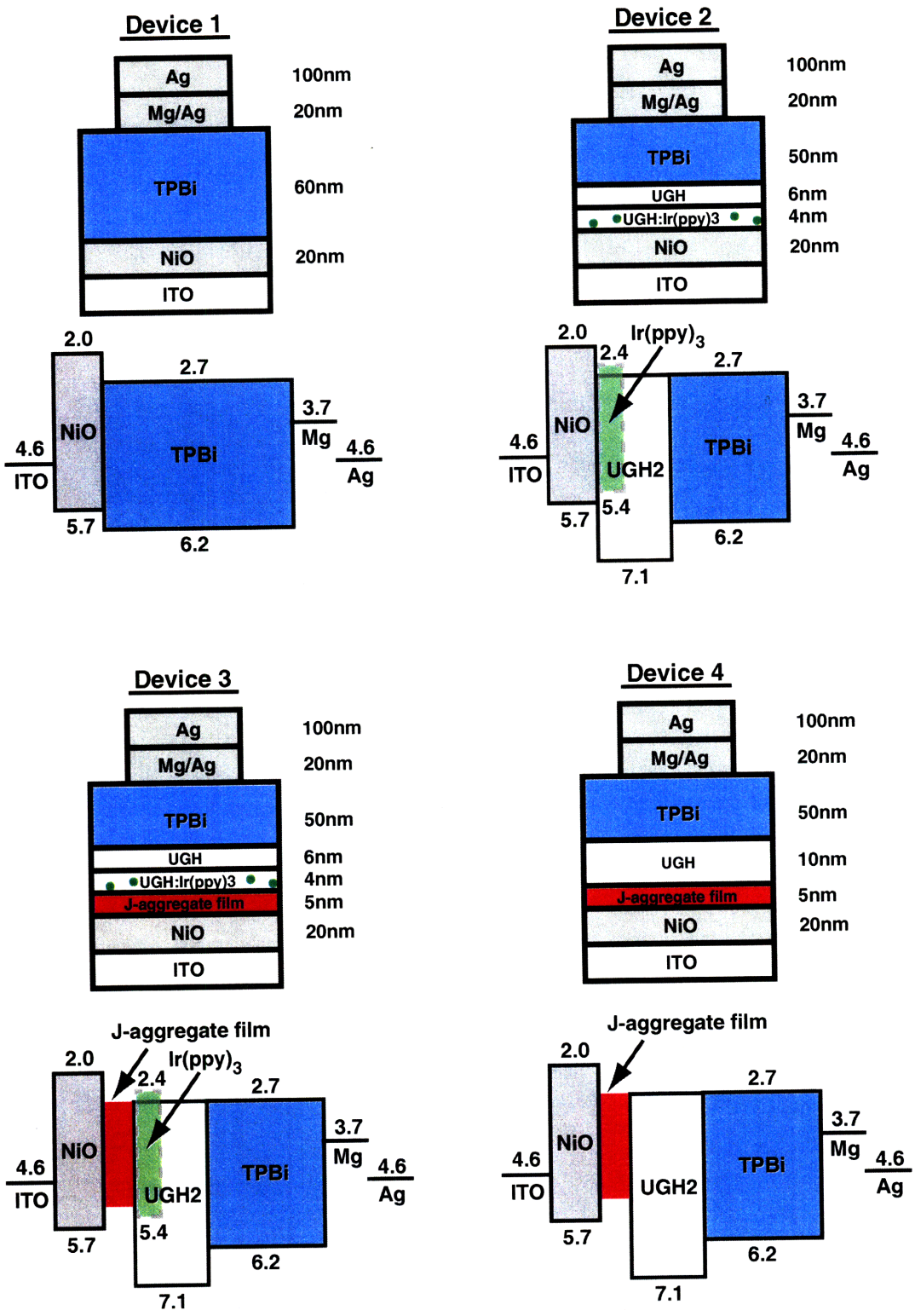

Figure 4-1: Device structures and their band diagrams of (a) Device 1: TPBi LED (b) Device 2: $Ir(ppy)_3$ LED (c) Device 3: JLED with FRET (d) Device 4: JLED without FRET

The four devices were tested unpackaged at room temperature and in ambient air. Figure 4-2 shows EL of the devices under forward bias. The luminescences were pictured from the substrate side of the devices. The substrates were covered with a shadow mask before evaporation of the cathodes, which defines 16 identical devices on each substrate. Only one device is turned on in each picture. The EL spectra for each of the four different structures are shown in Figure 4-3.

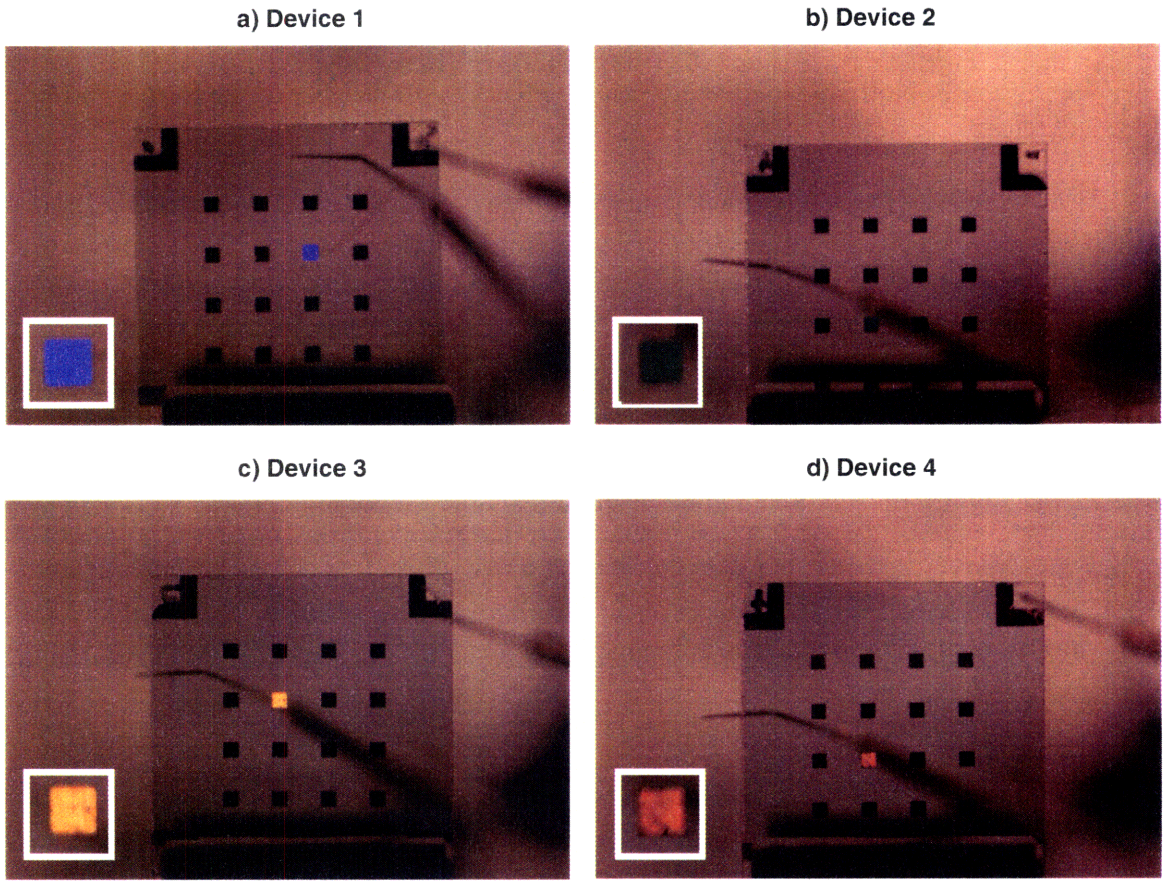

Figure 4-2: Device photos of (a) Device 1 at 8 volts (b) Device 2 at 19 volts (c) Device 3 at 9 volts (d) Device 4 at 10 volts.

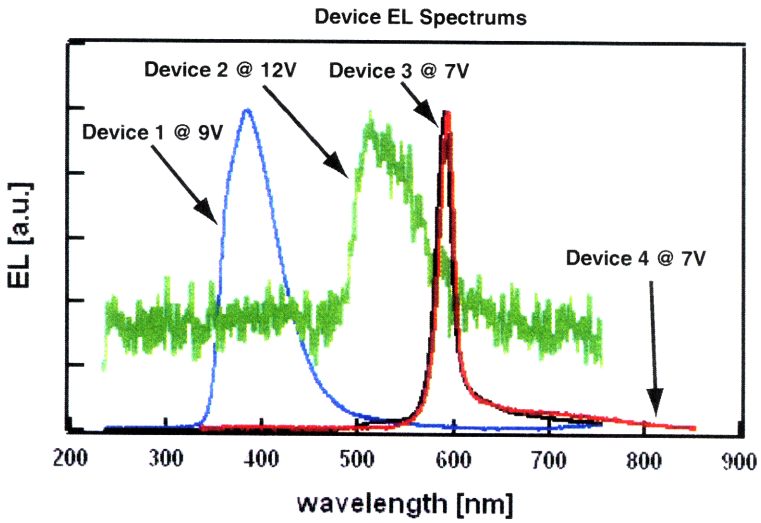

Figure 4-3: Normalized electroluminescence spectrums (EL) of the four devices

As expected, Device 1 shows a strong emission from TPBi. This emission is only observed from Device 1, indicating the effectiveness of UGH2 as the hole blocking layer in the other devices. Device 2 shows only weak EL, but its spectrum matches that of $Ir(ppy)_3$. Device 3 and Device 4 both show the narrow J-aggregate emission at 595nm. Device 3 is slightly blue shifted and has a small shoulder on the high energy side compared to Device 4. This is likely due to the unquenched $Ir(ppy)_3$ emission familiar from the energy transfer experiments in chapter two.

The external quantum efficiencies (EQE) of the devices are plotted in Figure 4-4. Each device is measured three times. These plots show instability in the film for all four devices, especially in Device 3 and 4. The efficiencies tend to decrease with the number of measurements performed. However, after the drastic decrease in efficiency from the first measurement, the films tend to be relatively stable. This is not a surprising result as the devices are composed of very different materials. Applying voltage across the device may rearrange the molecules into a more favorable configuration during the first measurement and hence change the morphology of the film. The maximum EQE of

Device 1, 2, 3 and 4 after the first measurement are 9E-4%, 1E-3%, 1E-3% and 6E-4% respectively. Device 3's EQE is ~1.7 times higher than Device 4's EQE, and although it is not definitive, we attribute the boost to the FRET.

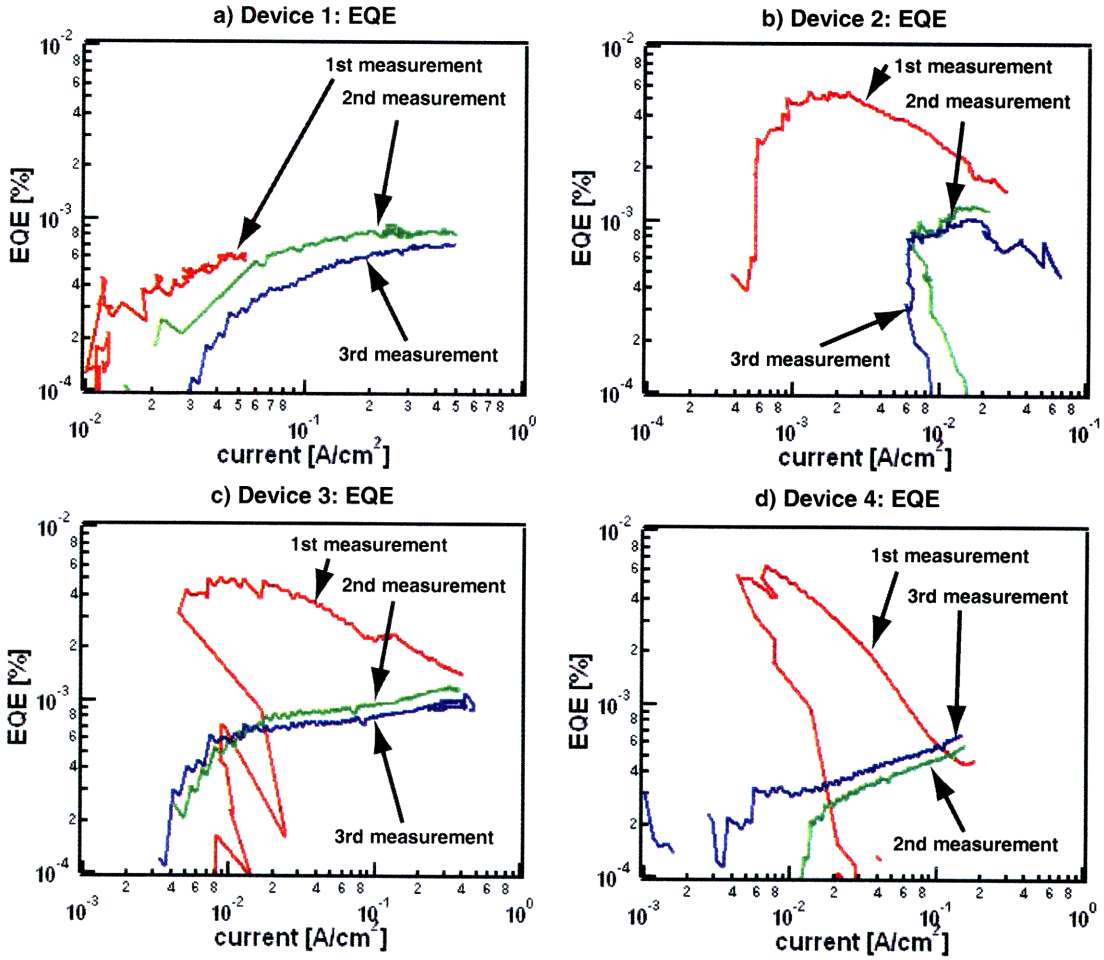

Figure 4-4: EQE curves of the four LEDs. Each device is measured three times consecutively.

An indication of FRET in Device 3 can also be seen in the I-V curves of the devices plotted in Figure 4-5. Again, each device is measured three times consecutively and the devices show stability after the first measurement. The similarity in the I-V characteristics between Device 3 and Device 2 rather than between Device 3 and Device 4 suggests that the J aggregate emission is mediated by exciton formation on $Ir(ppy)_3$.

Again, though it is not conclusive, FRET seems to play a major role in Device 3 as designed.

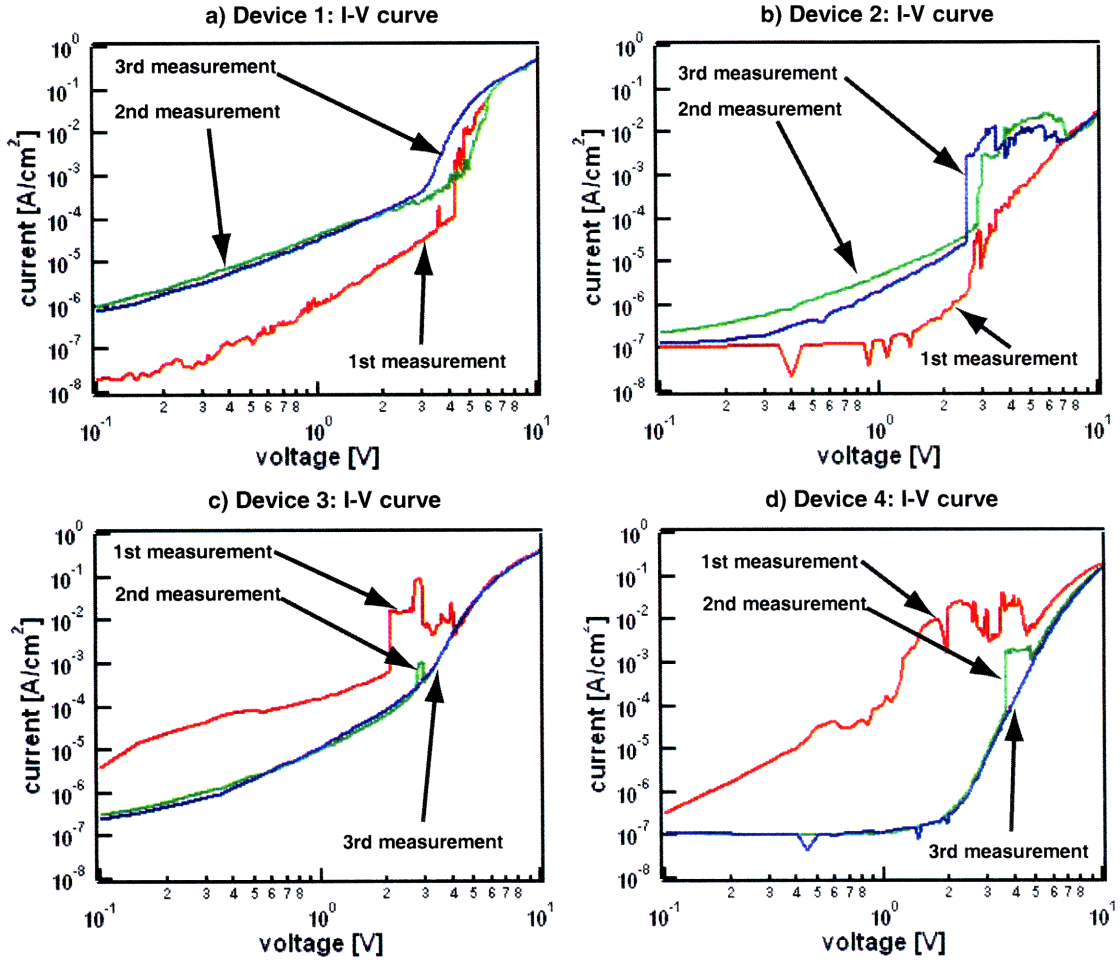

Figure 4-5: I-V curves of the four devices. Each device is measured three times consecutively.

4-2: Future Work

A novel JLED that incorporates metal oxide HTL was successfully demonstrated and the addition of the phosphor doping enhancing the EQE was shown. We attribute this enhancement to FRET between the phosphor and the J aggregates. These JLEDs, however, have very low quantum yield. Without changing the device structure, some ways to likely improve the efficiency are listed here.

1) Film uniformity is a crucial issue in making an efficient OLED because pillars in rough films may become sources of shortage in the device or aggregation of the materials. The surface treatment described in chapter two of this thesis was a successful attempt to abide by this rule when we brought two very different materials together. However, the roughness issue is also present in the interface between the NiO and the J aggregates. AFM images of 20nm of NiO grown on an ITO substrate and 4.5 BL J-aggregate film grown on the NiO is shown in Figure 4-6.

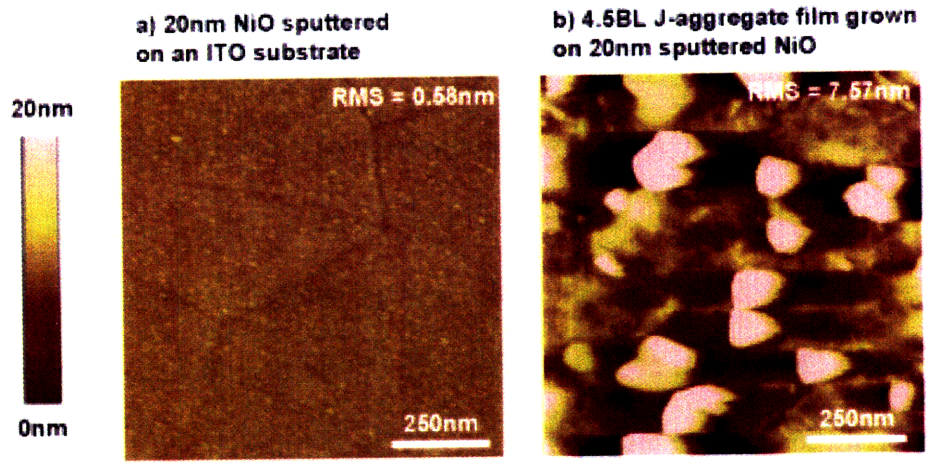

Figure 4-6: AFM images of (a) 20nm of sputtered NiO (b) 4.5 BL J-aggregate film grown on the sputtered NiO.

The AFM images cleary indicate that the J-aggregate film does not grow as uniformly on NiO substrate as it does on glass. This may limit device efficiency and cause some of the device instability. One possible solution to the problem is to grow fewer bi-layers of J-aggregate film. Another avenue of investigation is to grow the J-aggregate film at a different pH, as the J-aggregate dye solutions may etch the NiO.

2) Work by Jun Mei has shown sputtered SnO_2 can quench nearby tris-(8-hydroxyquinoline) aluminum (Alq_3) PL emission through FRET[32]. A similar quenching effect can be expected by our JLED device, for our emissive layer is placed adjacent to

NiO. A possible solution to the problem is to space the J-aggregate layer a few nanometers from the NiO which places the layer outside of the Förster radius. Another solution is, as discussed by Mei, to change the conductivity of NiO by adjusting the oxygen concentration while sputtering. This modifies the conductivity of the NiO, which in turn changes the Förster radius between the NiO and the J aggregates. By making the Förster radius small, the quenching effect can be minimized.

3) Despite UGH2's many useful properties for our energy transfer devices, UGH2 is not the best host for $Ir(ppy)_3$ when it comes to LEDs. UGH2's compatibility with the J-aggregate film after the surface treatment combined with its stability made it an excellent material choice in chapter two. UGH2 also serves as a good hole blocker when used in LEDs. However, as shown in Figure 4-1, the LUMO band of $Ir(ppy)_3$ is 0.3 eV higher than the LUMO band of UGH2. Despite holes getting captured by $Ir(ppy)_3$, the LUMO band offset makes the excitons hard to recombine on the $Ir(ppy)_3$ molecules. This band offset may explain some of the inefficiencies in Device 2. Since the efficiency of Device 3 relies on the J aggregates efficiently harvesting energy from $Ir(ppy)_3$ excitons, making Device 2 efficient will maximize the benefit from FRET. A solution may be to look for a different host material that still has the useful properties of UGH and also has the LUMO band higher than that of $Ir(ppy)_3$. Efficient exciton formations on the phosphor may also be achieved by choosing a different kind of phosphor that has its LUMO and HOMO bands lying between those of UGH2 and also permits FRET to J aggregates.

Chapter 5: Conclusion

This thesis demonstrated three main achievements: changing the surface chemistry of the TDBC J-aggregate thin films, confirming experimentally the Förster resonance energy transfer between $Ir(ppy)_3$ and the J aggregates, and building the J-aggregate light emitting devices that utilize the FRET. Each achievement is built on the achievement before.

The surface treatment in chapter two allows the J-aggregate films to be compatible with the evaporation of non-polar small molecules on top by making the hydrophilic surface of the film hydrophobic. This compatibility broadens the films' applications to not just LBL deposited devices but also to thermally evaporated devices. The FRET experiment in chapter three confirms the PL quenching and PL lifetime acceleration of $Ir(ppy)_3$ as predicted. Furthermore, the Förster radii calculated from the measurements were in good agreement with the theoretical R_F calculated from the spectral overlap. The JLED built in chapter four utilizes the FRET to enhance efficiency. The quantum efficiency and the I-V curves of the device suggest the presence of FRET.

Although the efficiency remains an issue, the JLED developed here can be readily incorporated into electrically pumped polaritonic devices.

Acknowledgement

First, I want to thank my thesis supervisor, Professor Vladimir Bulović, for providing this interesting project and being very supportive. I have learned so much from this project and it would not have been possible without him.

I want to thank Yaakov Tishler, Scott Bradley, Polly Anikeeva, and Vanessa Wood for sharing their time and knowledge to help me do various steps of this research. Yaakov and Scott have been a great source of knowledge on exciton-polaritons, J aggregates, and many other topics that went into this thesis. This project would not have come this far if it was not for their encouragements when my experiments seemed like they would never work. A great deal of physics education came from Polly's lectures on post-its. The energy transfer experiments would not have been so rewarding without her teachings and help with the experiments. Vanessa has been very helpful with the fabrication and measurements of the JLEDs. The JLED section of the research would not have been so smooth without her help.

I want to thank Steve Kooi and the Institute for Soldier Nanotechnologies for providing the setups for the time resolved PL measurements. These measurements were crucial to this project.

I want to thank Professor Arto Nurmikko and his group at Brown for conducting the pump probe measurements on the J-aggregate films. The video conferences with them also helped me learn more about the J aggregates.

I want to thank my JSU crew, Kimi, Kevin, Dan, Vic and others for being a good company on and off the basketball court during my stressful times. I enjoyed all the late night gatherings in the student center.

I want to thank my dad, mom, and brother for being very supportive throughout my life. None of this work would have been possible without their encouragements, financial support and unlikely knowledge in math, physics and optics.

Appendix A: Growth of a 5nm J-aggregate Thin Film

This section goes over the experimental details in making the TDBC J-aggregate thin film, which is used through out this research. It is one of the corner stones of the work and this research would not have been possible without it. The procedure given here was inspired by Fukumoto[14], tested and standardized with TDBC dye by Tischler[1] and further studied by Bradley[15].

The J-aggregate thin film was formed using the LBL method with a polyelectrolyte solution and a dye solution on a 1x1 inch glass substrate. The polyelectrolyte solution is poly(diallyldimethylammonium chloride) (PDAC), 20% by weight in water, M_w=400,000-500,000, obtained from Sigma-Aldrich (CAS 26062-79-3) and diluted to $3x10^{-2}$ M with deionized (DI) water. The dye used is 5,6-dichloro-2-[3-[5,6-dichloro-1-ethyl-3-(3-sulfopropyl)-2(3H)-benzimidazolidene]-1-propenyl]-1-ethyl-3-(3-sulfopropyl) benzimidazolium hydroxide, inner salt, sodium salt (TDBC) obtained from Nippon Kankoh Shikiso Kenkyusho Co., Ltd. (CAS 28272-54-0). $5x10^{-2}$ M solution of TDBC is made using DI water. PDAC and TDBC solutions are cationic and anionic solutions respectively and 400 mL of each are made in glass beakers. The solutions are prepared for LBL use by a recipe summarized in Table A-1. "Sonicate" refers to ultrasonic cleaning and "Stir" refers to stirring the solution using a one-inch magnetic spin bar. Care was taken so the TDBC solution did not get exposed to light.

Step	TIME [minutes]	TDBC	PDAC
1	20	Sonicate	Stir
2	10	Stir	Sonicate
3	20	Sonicate	Stir
4	5	Stir	Sonicate
5	5	Sonicate	Stir

Table A1: Recipe for preparing TDBC and PDAC solutions

The glass substrates were cleaned using the MIT LOOE standardized recipe summarized in Table A-2. The substrates were rinsed with DI water after Steps 1 and 2. After the 7th step, the substrates were treated with oxygen plasma for six minutes with a Plasma Preen system.

Step	Time [minutes]	Description
1	5	Sonicate in detergent (Micro-90)
2	5	Sonicate in DI water
3	5	Sonicate in DI water (different water)
4	2	Sonicate in acetone
5	2	Sonicate in acetone
6	2	Sit in boiling isopropynal (IsoP)
7	2	Sit in boiling isopropynal (different IsoP)

Table A-2: Recipe for cleaning the glass substrates

After the substrates were cleaned and the solutions were prepared, LBL was performed using an automated Leica Autostainer XL. The dipping steps for one SICA of LBL are summarized in Figure A-1. The process is repeated 4.5 times to form 4.5 bi-layer (BL) J-aggregate thin films. The last 0.5 times refers to immersion into the PDAC solution followed by the three rinses. Analysis by Bradley shows that 4.5 BL film is 5.1 nm thick.

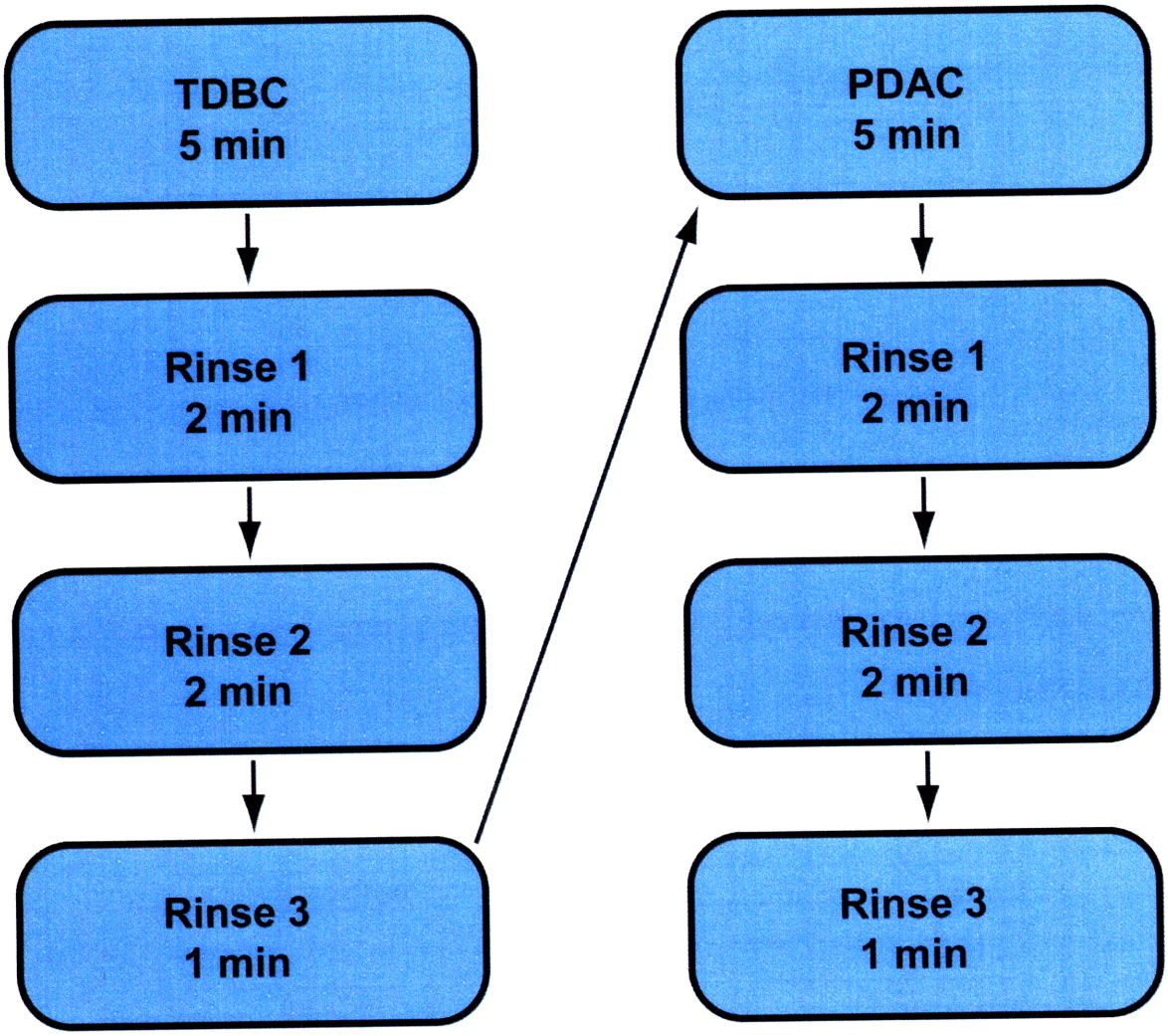

Figure A-1: Dipping procedure for J-aggregate thin film LBL growth

After the films were fished out of the stainer, they were blown dry with nitrogen gas. Since the film forms on both sides of the substrate, one of the sides was wiped off clean using TexWipe soaked with methanol. The absorption and emission spectrums of a 4.5 BL J-aggregate film are shown in Figure A-2.

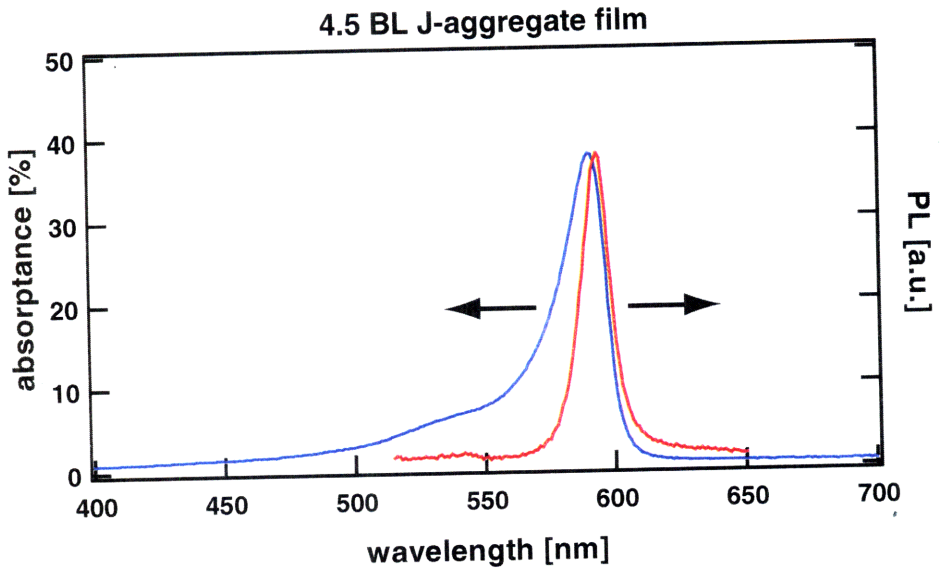

Figure A-2: The absorption and emission spectrums of a 4.5 BL J-aggregate film.

The absorption spectrum was obtained by subtracting reflection and transmission spectrums of 4.5 BL J-aggregate film from 100%. The reflection and transmission spectrums were measured using Cary 500i and Cary 5E spectrometer respectively. The PL spectrum was obtained by exciting the film at 500nm and using a detector to collect the emission. The high absorption peak and the narrow linewidth are the characteristics of J-aggregation.

Appendix B: Theoretical Förster Radius Between an $Ir(ppy)_3$ Molecule and a TDBC J Aggregate

The Förster radius, R_F, between an $Ir(ppy)_3$ molecule and a J aggregate is given by:

$$R_F^6 = \frac{3}{4\pi}\frac{c^4}{n^4}\eta_D \int_{-\infty}^{\infty} \frac{S_D(\omega)\sigma_A(\omega)}{\omega^4} d\omega \qquad \text{(Eq. B-1)}$$

where c is the speed of light in vacuum and n is the index of refraction of the medium between the donor and acceptor molecules. The index of the medium used here, UGH2, is 1.7. The value, which is typical for organics, was obtained from ellipsometry of 50 nm of UGH2 on a crystalline silicon substrate. η_D is the internal quantum efficiency of the donor and 0.15 is used for $Ir(ppy)_3$ [22]. $S_D(\omega)$ is the donor emission spectrum normalized over angular frequency, ω. σ_A is the acceptor absorption cross-section of the acceptor. σ_A is found from applying the Beer-Lambert Law to the absorption measurements of the 4.5 BL J-aggregate film (5.1 nm). The Beer-Lambert Law is

$$I_t(\omega) = I_i(\omega)e^{-\sigma_A(\omega)Nl} \qquad \text{(Eq. B-2)}$$

where $I_t(\omega)$ is the intensity of transmitted light through a film, $I_i(\omega)$ is the intensity of the light before entering the film, N is the density of the J aggregates in the film, and l is the thickness of the film. From the pump probe experiment at Brown University by the Arto Nurmikko group and absorption experiments of TDBC monomers in solution by Tischler and Bradley, N is estimated to be 0.5 aggregates/nm^3.

As obvious from Eq. B-1, one of the important factors that determine the Förster radius is the spectral overlap of the donor emission and the acceptor absorption spectrums. The normalized emission spectrum of $Ir(ppy)_3$ and the absorption cross-section of TDBC J aggregates are shown in Figure B-1. Although the two spectrums have their peaks at different wavelengths, they show relatively good overlap otherwise. From Eq. B-1 the Förster radius is calculated to be 3.84 nm

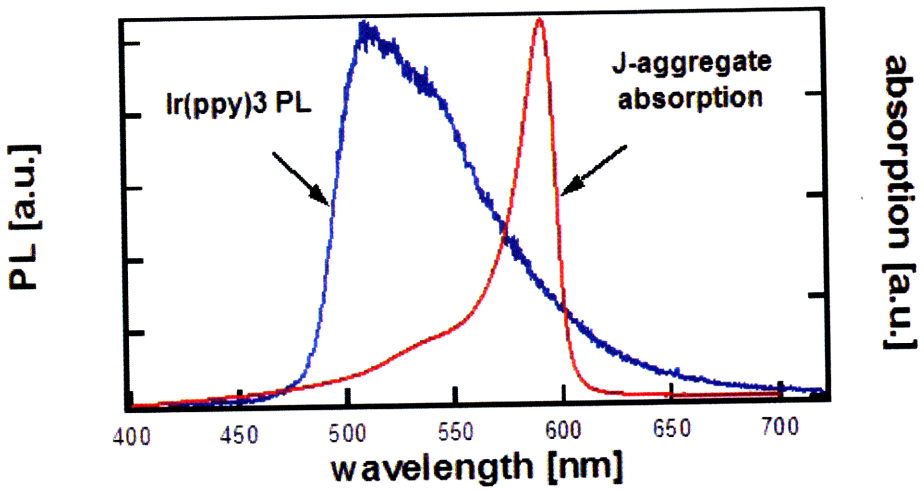

Figure B-1: The emission spectrum of the donor, $Ir(ppy)_3$, and the absorption spectrum of the acceptor, J aggregates.

There are many other kinds of cyanine dye molecules that form J aggregates with absorption peaks at different wavelengths and they were considered as well for the experiment. However, a simulation shows that shifting the TDBC J-aggregate absorption spectrum does not improve the overlap by more than two folds. Since the Förster radius is proportional to the sixth root of the spectral overlap, the two-fold increase does not have a considerable effect on the radius. The negligible difference makes TDBC as good a candidate for the FRET experiment as any other kind of cyanine dye.

Appendix C: Different Attempts to Surface Treat the J-aggregate film

In the attempt to make the J-aggregate film surface hydrophobic, there were two alternative methods that were experimented. These methods seemed as logically sound as the method presented in chapter two but they did not produce the desired outcome. One method is to apply anionic surfactant such as sodium dodecyl sulfate (SDS) directly on the positively charged surface of the 4.5 BL J-aggregate film. Another method is to end the J-aggregate film growth with 4 BL to charge the surface negative and then use the cationic surfactant.

The first method does succeed in making the surface hydrophobic. When the film is immersed in 0.01 M SDS solution for 1 minute, the contact angle is increased to ~40°. However, aside from the treatment not being as effective as the CTAB treatment, the immersion "kills" the J-aggregate film. The color of the film dims significantly. From experience, this is attributed to the SDS molecules replacing the TDBC molecules which are only weakly bonded to the PDAC polymers.

The second method only yields a contact angle of ~18° which is practically the same as that of an untreated 4.5 BL J-aggregate film. This is attributed to 4 BL films not having many charged sites for CTABs to bond to. Since TDBC molecules only have two bonding sites per molecule, the next layer in LBL does not adsorb unless it is polymers with multi-valent sites. For this reason, CTAB, which only has one bonding site per molecule, does not adsorb well.

Bibliography

[1] J. R. Tischler. Solid State Cavity QED: Practical Applications of Strong Coupling of Light and Matter. Doctoral thesis, Massachusetts Institute of Technology, **2007**.

[2] J. McKeever, A. Boca, A. D. Boozer, J. R. Buck, and H. J. Kimble, *Nature* **2003**, 425, 268.

[3] M. Saba, C. Ciuti, J. Bloch, V. Thierry-Mieg, R. Andre, Le Si Dang, S. Kundermann, A. Mura, G. Bongiovanni, J. L. Staihli, B. Deveaud, *Nature* **2001**, 414, 731.

[4] C. Monroe, *Nature* **2002**, 416, 238.

[5] J. R. Tischler, M. S. Bradley, V. Bulović, J. H. Song, A. Nurmikko, *Phys. Rev. Lett.* **2005**, 036401.

[6] E. E. Jelley, *Nature* **1936**, *138*, 1009.

[7] G. Scheibe, *Z. Angew. Chem.* **1936**, *49*, 563.

[8] J. Knoester, *International Journal of Photoenergy* 2006, 61364, 1.

[9] D. G. Lidzey, D. D. C. Bradley, M. S. Skolnick, T. Virgili, S. Walker, D. M. Whittaker, *Nature* **1998**, 395, 53.

[10] P. Kelkar, V. Kozlov, H. Jeon, A. Nurmikko, C.-C. Chu, D. C. Grillo, J. Han, C. G. Hua, R. L. Gunshor, *Phys. Rev. B* **1995**, 52, R5491.

[11] P. A. Hobson, W. L. Barnes, D. G. Lidzey, G. A. Gehring, D. M. Whittaker, M. S. Skolnick, S. Walker, *Appl. Phys. Lett.* **2002**, 81, 3519.

[12] D. F. O'Brien, *Photo. Sci. Eng.* **1974**, *18*, 16.

[13] K. Misawa, H. Ono, K. Minoshima, T. Kobayashi, *Appl. Phys. Lett.* **1993**, *63*, 577.

[14] H. Fukumoto, Y. Yonezawa, *Thin Solid Films* **1998**, *327-329*, 748.

[15] M. S. Bradley, J. R. Tischler, V. Bulović, *Adv. Mater.* **2005**, 17, 1881.

[16] G. Decher, J. D. Hong, *Makromol. Chem., Macromol. Symp.* **1991**, *46*, 321.

[17] K. Ariga, Y. Lvov, T. Kunitake, *J. Am. Chem. Soc.* **1997**, *119*, 2224.

[18] D. Dexter, T. Förster, R. Knox, *Phys. Status solidi* **1969**, 34, K159.

[19] T. Förster, *Annalen der Physik* **1948**, 6, 55.

[20] M. A. Baldo, D. F. O'Brien, Y. You, A. Shoustikov, S. Sibley, M. E. Thompson, S. R. Forrest, *Nature* **1998**, 395, 151.

[21] C. Adachi, M. A. Baldo, M. E. Thompson, S. R. Forrest, *J. Appl. Phys.* **2001**, 90, 5048.

[22] P. O. Anikeeva, C. F. Madigan, S. A. Coe-Sullivan, J. S. Steckel, M. G. Bawendi, V. Bulović, *Chem. Phys. Lett.* **2006**, 424, 120.

[23] X. Ren, J. Li, R. J. Holmes, P. I. Djurovich, S. R. Forrest, M. E. Thompson, *Chem. Mater.* **2004**, 16, 4743.

[24] P. Andrew, W. L. Barnes, *Science* **2000**, 27 785.

[25] P. T. Hammond, *Adv. Mater.* **2004**, 16, 1271.

[26] M. A. Baldo, M. E. Thompson, S. R. Forrest, *Nature* **2000**, 403, 750.

[27] Collaboration with Brown University, Q. Zhang, T. Atay, A. Nurmikko **2006**.

[28] J.-M. Caruge, J. E. Halpert, V. Bulović, M. G. Bawendi, *Nano Lett.* **2006**, 6, 2991.

[29] D. Ragone, *Thermodynamics of Materials Volume II.* John Wiley & Sons. Inc., New York, 1995.

[30] V. Wood. All Inorganic Colloidal Quantum Dot LEDs. Master's thesis, Massachusetts Institute of Technology, **2007**

[31] H. J. Bolink, E. Coronado, D. Repetto, M. Sessolo, E. M. Barea, J. Bisquert, G. Garcia-Belmonte, J. Prochazka, L. Kavan, *Adv. Funct. Mater.* **2008**, 18, 145.

[32] J. Mei. Photoluminescence Quenching of Organic Thin Films by Transparent Conductive Oxides. Senior thesis, Massachusetts Institute of Technology, **2006**.